AGU100 ADVANCING EARTH AND SPACE SCIENCE

Tectonics

RESEARCH ARTICLE
10.1029/2018TC005112

Special Section:
Geodynamics, Crustal and Lithospheric Tectonics, and active deformation in the Mediterranean Regions (A tribute to Prof. Renato Funiciello)

Key Points:
- We identify four different rotational domain in the Central Tauride intramontane basins
- The restoration of the rotational domains predicts a minimum NE-SW horizontal extension of ~30–35 km across the basin system
- The Sultandağları range may represent a Miocene extensional core complex

Supporting Information:
- Supporting Information S1
- Data Set S1

Correspondence to:
A. Koç,
aytenkoc@yyu.edu.tr;
a.koc@uu.nl

Citation:
Koç, A., van Hinsbergen, D. J. J., & Langereis, C. G. (2018). Rotations of normal fault blocks quantify extension in the Central Tauride intramontane basins, SW Turkey. *Tectonics*, *37*, 2307–2327. https://doi.org/10.1029/2018TC005112

Received 18 APR 2018
Accepted 27 JUN 2018
Accepted article online 4 JUL 2018
Published online 3 AUG 2018

Rotations of Normal Fault Blocks Quantify Extension in the Central Tauride Intramontane Basins, SW Turkey

Ayten Koç[1], Douwe J. J. van Hinsbergen[2], and Cor G. Langereis[2]

[1]Department of Geological Engineering, Van Yüzüncü Yıl University, Van, Turkey, [2]Department of Earth Sciences, Utrecht University, Utrecht, Netherlands

Abstract Quantifying the amount of stretching in extensional basin systems is often challenging in the absence of seismic profiles or boreholes. However, when fault spacing and orientation as well as vertical axis rotation patterns are known, map-view restoration may provide a good estimate of total extension. This integrated structural and paleomagnetic approach provides a relatively straightforward tool in extensional basin restoration and fault zone kinematic analysis. Here we provide results of an extensive paleomagnetic survey of the Neogene Central Tauride intramontane basins (SW Turkey), where previous work revealed a complex array of basin-bounding normal faults and relay ramps. In total, 437 oriented cores were sampled at 43 sites distributed within Miocene-Pliocene continental sedimentary rocks from the Ilgın, Altınapa, Yalvaç, and Beyşehir basins. Despite the more or less coherent overall strike of the mountain belt and basins, rotations vary from ~42° clockwise (Yalvaç) to ~10° (Beyşehir), ~21° (Ilgın), and ~30° (Altınapa) counterclockwise. We show that the rotation pattern is related to normal faults and lateral variations in fault displacement superimposed on regional rotation patterns. We restore these to estimate a minimum NE-SW horizontal extension of ~30–35 km across the basin system. As a consequence of our reconstruction, it appears that the Sultandağları range that exposes low-grade metamorphic Paleozoic and Mesozoic rocks of the Geyikdağı and Bolkardağ nappes of the Taurides represents a Miocene extensional core complex.

1. Introduction

The amount and rate of extension is an important parameter in assessing physical properties of sedimentary basins (Jarvis & Mckenzie, 1980). In smaller basin systems, estimates may be derived from calculating individual normal fault throws if offset markers are constrained, for example, through seismic profiles or borehole data (Gibbs, 1983; Jackson, 1987). In the many occasions where such data are unavailable, however, estimating normal fault displacement is challenging, because displaced markers are buried in hanging walls and may be eroded in footwalls.

An alternative and indirect approach to arrive at first-order estimates of extension is by integrating structural analysis with paleomagnetic analysis of vertical axis rotation patterns. Extensional basins are often laterally discontinuous, and within (half-)grabens, normal fault systems are often segmented, whereby segments are connected through relay ramps (e.g., Larsen, 1988; Ori, 1989; Peacock, 2002; Peacock & Sanderson, 1994; Trudgill & Cartwright, 1994). Such systems, developing at the scale of laterally discontinuous (half) grabens or at the scale of individual normal fault segments, are associated with lateral strain variations, which lead to vertical axis rotations. On a regional scale, lateral variation in regional back-arc basin extension led to major opposite forearc block rotations in, for example, the Aegean region (van Hinsbergen & Schmid, 2012) or the Sea of Japan (e.g., Martin, 2011). On a smaller scale, vertical axis rotations may result from lateral displacement variations on individual faults (Sussman et al., 2004).

Behavior of fault-bounded crustal units may vary from rigid, discrete blocks to regionally uniformly distributed shear. In the case of rigid blocks that remain internally undeformed, strain is accommodated by slip at bounding fault zones and rotation is accommodated by laterally varying displacements along bounding faults (Nelson & Jones, 1987). This model is best applicable to upper crustal, brittle deformation on the scale of individual basins, where the main faults and intervening undeformed blocks are mapped. On larger scale, for example, of large basin complexes, an alternative approach is to abandon the concept of rigidity and use a

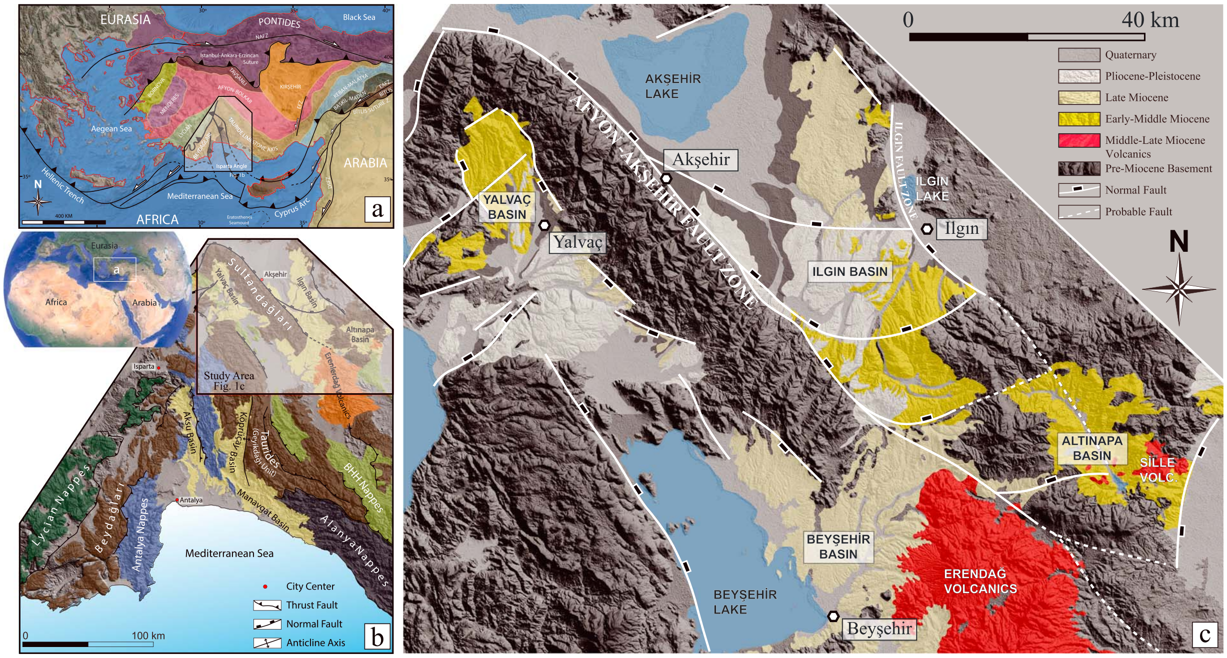

Figure 1. (a) Simplified structural map with the major tectonic zones of Turkey overlain on a Shuttle Radar Topography Mission (SRTM) topographic image. (b) Major tectonic structures and units in the Isparta angle. (c) Simplified geological map of the study area.

continuum description for deformation (McKenzie & Jackson, 1983). In both approaches, blocks within a single domain rotate by the same amount in the same direction (Garfunkel & Ron, 1985; McKenzie & Jackson, 1983; Ron et al., 1984).

Vertical axis rotation analysis may thus help to quantify the amount of regional horizontal strain variations. These relative variations may either provide minimum estimates of total strain across a region and may be converted to total strain if calibrated in one location (e.g., where no deformation occurred, on a lateral edge of an extensional domain). Different senses of vertical block rotation, either clockwise (CW) or counterclockwise (CCW) within a single domain may further help to find style and amount of deformation.

A wide extensional domain hosting the Neogene Central Tauride intramontane basins (CTIB) in SW Turkey is an example of a probably relatively low-strain extensional region where the total amount of extension remains unquantified. Simultaneously with the formation of these basins, a westward convex orocline formed in the Central Taurides (Koç, van Hinsbergen, et al., 2016). This oroclinal bending was associated with several tens of kilometers of shortening to the west and has been attributed to be caused by an isolated *Antalya* slab (Biryol et al., 2011; van der Meer et al., 2018) that may or may not still be connected to the Bey Dağları foreland of SW Turkey (Koç, van Hinsbergen, et al., 2016). The CTIB to the east of the orocline may balance the shortening in the front such that the oroclinal bending was associated with no net displacement between Central and Western Turkey (Figures 1a and 1b). To test this, however, a quantification of Miocene extension in the CTIB is required.

The CTIB hosts a series of Mio-Pliocene continental extensional sedimentary basins, including the Beyşehir, Yalvaç, Ilgın, and Altınapa basins, which are located in the hanging walls of major normal fault systems that are structurally well mapped (Koç et al., 2017; Koç, Kaymakci, et al., 2016; Koç et al., 2012; Koçyiğit & Özacar, 2003; Figure 1c). The present-day tectonic regime in these continental basins shows that the region experiences active extension, as portrayed by active seismicity, earthquake focal mechanisms, field data including fault plane solutions, and GPS measurements (Kalyoncuoğlu et al., 2011; Koç et al., 2017; Koç, Kaymakci, et al., 2016; Koç et al., 2012; Koçyiğit & Özacar, 2003; Reilinger et al., 2006; Figure 2). Basin analysis revealed that the modern extensional regime in these continental basins started in at least Middle Miocene times and probably already in the Early Miocene when the first sediments started accumulating (Koç et al., 2017; Koç, Kaymakci, et al., 2016; Koç et al., 2012). What makes these basins particularly complex is that bounding normal fault

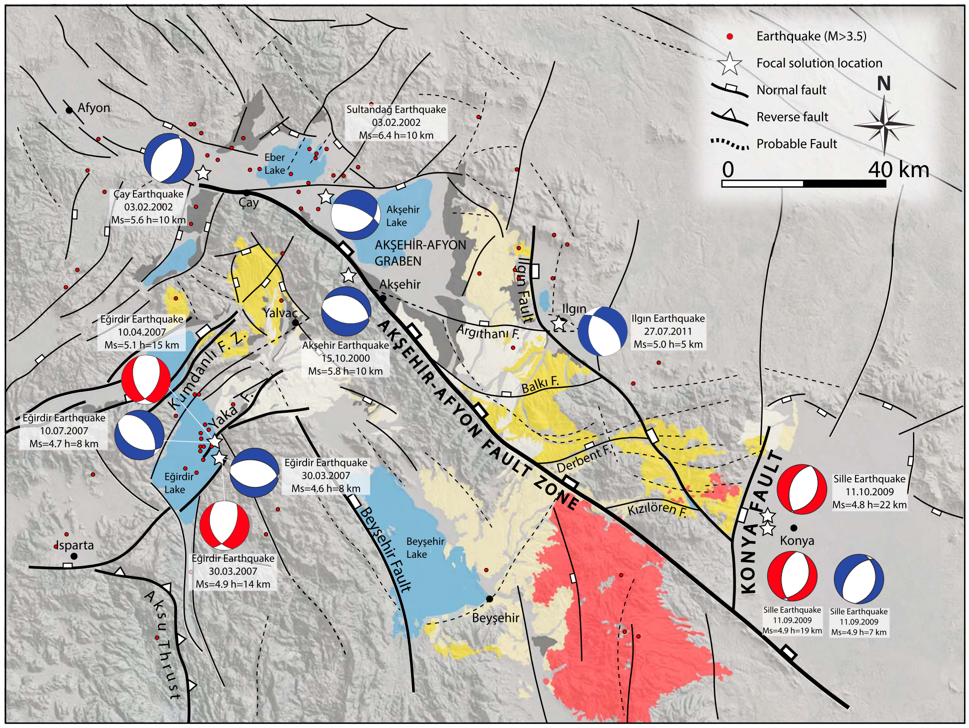

Figure 2. Major structures of the region are shown on a shaded relief image, with moment tensor solutions of the recent major earthquakes. Beach balls with red show focal mechanism solutions from Harvard Global Centroid Moment Tensor (CMT) catalog, and beach balls with blue indicate focal mechanism solutions from Ergin et al. (2009), Taymaz et al. (2004), Poyraz et al. (2014), Earthquake Research Department (ERD, Ankara), and Institute of Tchnology (ETH) of Zurich (ETHZ) catalogs. Label for earthquake mechanism indicates date, magnitude, and hypocenter depth.

systems are multidirectional and strike at angles of ~90° to each other, and on the scale of the basins, multidirectional, dominantly NE-SW and NW-SE extension prevailed from the Miocene to the present (Koç et al., 2017; Koç, Kaymakci, et al., 2016; Koç et al., 2012).

Here we provide results of an extensive paleomagnetic study constraining vertical axis rotation in the Beyşehir, Yalvaç, Ilgın, and Altınapa basins since the Miocene. We integrate the results with constraints on normal fault geometry, pattern, and evolution to arrive at a first-order map-view reconstruction that allows estimating horizontal extension in the study area. We discuss these results within the context of the tectonic and geodynamic evolution of the Central Tauride region and illustrate the general use of paleomagnetic constraints in estimating crustal extension by restoring tectonic rotations.

2. Geological Setting and Structural Geological Constraints

Complex deformation in Anatolia is caused by long-lived convergence between Africa and Eurasia since the Cretaceous (Figure 1a). The convergence was accommodated by northward subduction at multiple subduction zones that consumed a complex paleogeography of continental platforms and basins collectively referred to as the Adria-Turkey Plate (Stampfli et al., 1991) or Greater Adria (Gaina et al., 2013), of which the Anatolian part is referred to as the Anatolide-Tauride block (s) (Barrier & Vrielynck, 2008; Dewey & Şengör, 1979; Gürer et al., 2016; Okay, 1986; Pourteau et al., 2010; Robertson, 2004; Şengör & Yılmaz, 1981; van Hinsbergen et al., 2016). The İzmir-Ankara-Erzincan suture zone runs along the southern margin of Pontides, which have been part of Eurasia since at least mid-Mesozoic time, and marks the former position of the Northern Branch of the Neotethys (Şengör & Yılmaz, 1981). A second subduction zone originated within the Neotethys ocean to the north of the (Anatolide)-Taurides in Late Cretaceous time. It accommodated subduction of the continental lower crust during the latest Cretaceous to Eocene during which time continental upper crust was stacked into the Taurides fold-thrust belt. The Taurides and Africa were separated by this subsequently consumed oceanic lithosphere of the Southern Branch of the Neotethys (Gürer et al., 2016; Menant et al., 2016; van Hinsbergen, Kaymakci, et al., 2010; van Hinsbergen et al., 2016). This subduction zone is still active today along the Cyprus subduction zone to the west of the island of Cyprus (Granot, 2016; Khair & Tsokas, 1999). Anatolia is located on the overriding plate of this complex subduction system with bow-like trenches forming at the junction of Aegean and Cyprus *arcs* (Figure 1a). In Eastern Turkey, this Southern Branch has been entirely subducted and is demarcated by the Bitlis suture zone, with the arrest of subduction at the end of the Middle Miocene (Faccenna et al., 2006; Hüsing et al., 2009; Keskin, 2003; Okay et al., 2010; Şengör et al., 2003; Şengör & Yılmaz, 1981). Subduction along the Cyprus arc is in its latest stages, and subduction of the stretched African continental margin and overlying Cretaceous obducted ophiolitic klippen has occurred since the Late Miocene on Cyprus and was probably associated with slab break-off since the Middle Miocene (Biryol et al., 2011; Faccenna et al., 2006; Gans et al., 2009; Schildgen et al., 2014; van der Meer et al., 2018). To the west, the Antalya slab is located below the Bay of Antalya, is separated by a gap from the Cyprus slab (Biryol et al., 2011; van der Meer et al., 2018), and may have been decoupled from the African plate since the Eocene.

During this intense deformation history of shortening, a fold and thrust belt formed a carbonate-dominated mountain range in southern Turkey, with dominantly south (west) ward thrusting until Late Eocene time (Altıner et al., 1999; Andrew & Robertson, 2002; Mackintosh & Robertson, 2009; Meijers et al., 2011; Özer et al., 2004; Ricou et al., 1975). The belt shows major large-displacement thrusts and smaller-scale duplexes and imbricates, and today its high topography (at elevations up to 2,200 m) is covered by Neogene sedimentary basins (Figures 1b and 1c). These basins formed in the upper plate above the Cyprus and Antalya slabs and were filled by marine to continental sediments and volcanics. The dominantly marine basins (Aksu, Manavgat, and Küprüçay basins, Figure 1b) are located mainly in the central and southern limb of the belt while the continental basins started to form in the north, since the Early Miocene. These intramontane basins include the Altınapa, Yalvaç, Ilgın, and Beyşehir basins (Figure 1c), which are the main concern of this study. The stratigraphy of the Altınapa basin is displaying Early Miocene fining upward fluvio-lacustrine sediments (which we name the lower Altınapa unit), unconformably overlain by Middle Miocene lacustrine and volcaniclastic sediments, as well as andesitic lavas (upper Altınapa unit). $^{40}Ar/^{39}Ar$ dating from volcaniclastic levels provide 11.8–11.6 Ma ages and the main basin forming phase occurred prior to 11.8 Ma (Koç et al., 2012). The Ilgın basin (IB) shows a similar stratigraphy with the earliest age recorded in Early Miocene lacustrine deposits at Harami (Krijgsman et al., 1996). These deposits are the distal equivalent of Early Miocene red clastic deposits in the western edge of the IB. These red clastics are uncomformably overlain by Middle Miocene lacustrine deposits (Koç et al., 2017). This age is also supported by the radiometric age determinations from pumice deposits in the stratigraphy of the IB (11.61 Ma). A similar stratigraphy was recently documented from the Yalvaç basin (YB) with the clearest depocenter represented by Middle Miocene fine-grained lacustrine deposits (Koç, Kaymakci, et al., 2016). The onset of sedimentation in the YB is not known precisely, but available biostratigraphic control shows that it must have started during or before the Middle Miocene. The Beyşehir basin (BB) also contains lacustrine sediments and volcanics, and these comprise the youngest deposits we sampled, with the Early Miocene-Pliocene age (Keller et al., 1977; Tatar et al., 2002).

The major (normal) faults bounding these continental basins are the Beyşehir fault bordering the west side of Beyşehir Lake and BB, the major Aksehir-Afyon fault zone bordering the western limit of the IB (Figure 2). These major faults also governed basin formation, with proximal facies close to the basin margins and basinward grading into lacustrine deposits, representing local depocenters. Between the Aksehir-Afyon fault zone and Ilgın fault a number of E-W trending normal faults have been documented (Koç et al., 2017) (Figure 2) that redistribute the strain laterally and connect to these major faults through relay ramp geometry. Paleostress inversion analysis based on growth faults shows that the basins formed during multidirectional extension, with NE-SW to E-W extension dominating over subordinate N-S extension (Koç et al., 2017).

Despite the long and intense history of shortening caused by Africa-Europe convergence, the present-day tectonic regime as portrayed by active seismicity, earthquake focal mechanisms, field data, including fault plane solutions, and GPS measurements shows that these basins experienced extension, and extension-related subsidence is controlled by these basin bounding faults. Focal mechanism solutions of moderate-size earthquakes in historic times along the major faults indicate regionally multidirectional extension, with the range-bounding major normal faults accommodating dip-slip NE-SW extensions that occur in tandem with NW-SE extension accommodated along less prominent fault zones (Ergin et al., 2009; Koç et al., 2017; Poyraz et al., 2014; Taymaz et al., 2004; Tiryakioğlu et al., 2013; Figure 2).

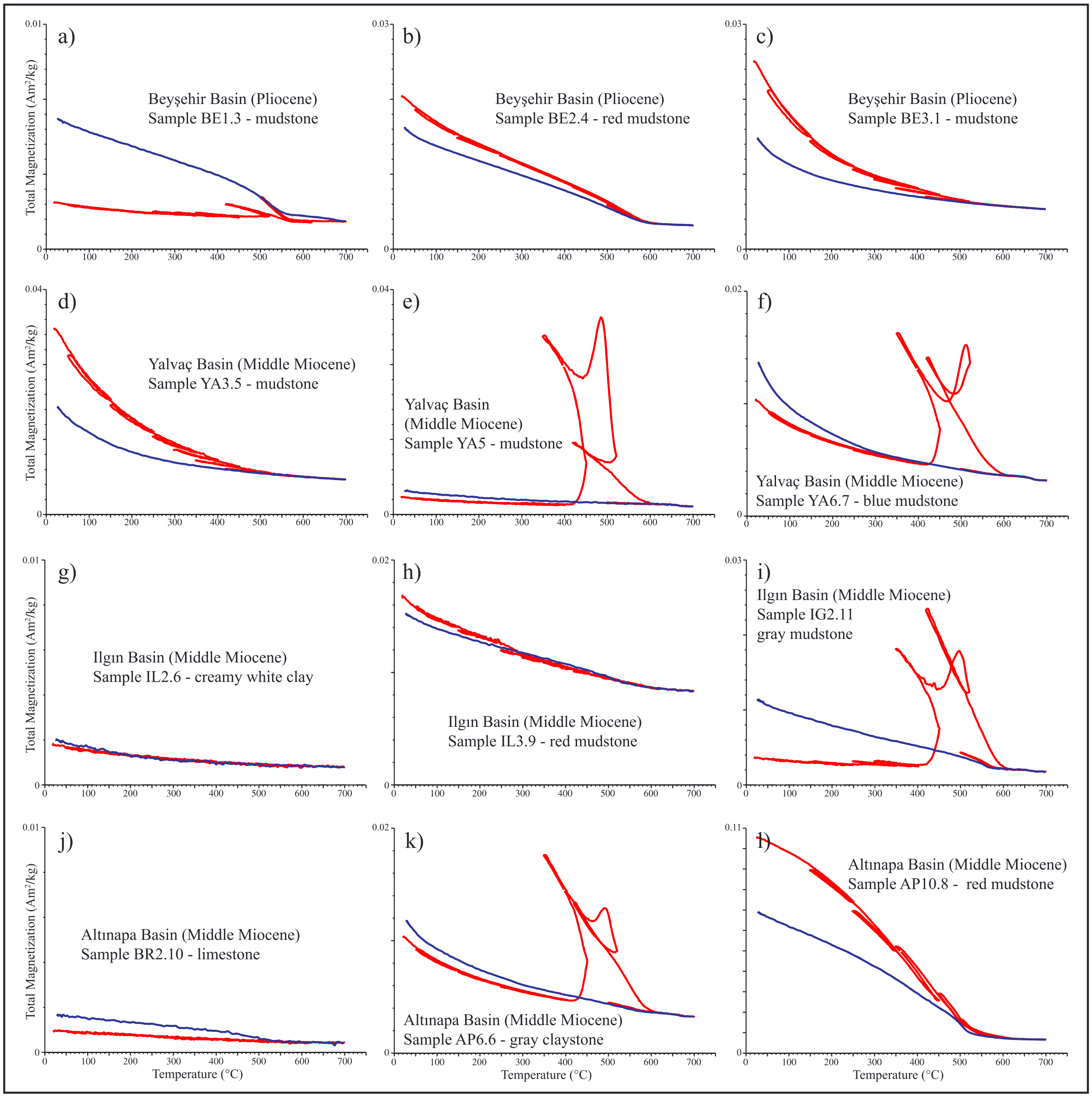

Figure 3. Thermomagnetic curves using six heating and cooling cycles (red lines) up to 700 °C for representative samples. The final cooling segment (blue line) is indicated with a thicker line. A noisy appearance is indicative of a weak magnetic signal. See text for explanation of the thermomagnetic behavior.

3. Paleomagnetic Sampling and Analysis

In total, 437 oriented cores were sampled at 42 sites distributed within Miocene-Pliocene continental (mostly lacustrine) sedimentary rocks from the CTIB at the eastern limb (Ilgın and Altınapa basins) and central part (Yalvac and Beyşehir basins) of the Isparta angle. We sampled fresh sedimentary rock in exposures away from major brittle faults to minimize rotations reflecting local deformation. From the IB 12 sites were sampled, 17 sites come from the Altınapa basin, 8 sites were collected from the YB, and 5 from the BB (Figures 2 and 6). Samples were taken from limestones, silt, and claystones, and from a few tuffs deposited in lacustrine environments. Samples were drilled using a gasoline powered motor drill, and sample orientations were measured with a magnetic compass. Sample orientations as well as bedding attitudes were corrected for present-day declination (+4.5°). At least 10 standard oriented cores were collected from each site after removing the weathered surface of the outcrop. In the laboratory, samples were cut into standard specimens, providing in most cases two or more specimens per core (referred to as A and B specimens, for deeper and shallower parts of the core, respectively).

To determine magnetic carriers of the ChRM in the samples, thermomagnetic runs were carried out in air (Figure 3), using a modified horizontal translation-type Curie balance, with a sensitivity of ~5 × 10–9 Am^2 (Mullender et al., 1993). Approximately 50–100 mg of powdered rock sample (depending on the magnetic intensity of the sample) was put into a quartz-glass sample holder held in place by quartz wool. The measurement procedure consists of six heating and cooling cycles up to a maximum of 700 °C with 10 °C/min rates.

Approximately 660 specimens were demagnetized (Table 1). Thermal stepwise demagnetization of ~440 specimens was performed in (20–30°) temperature steps from room temperature up to 400–680 °C (depending on the maximum unblocking temperature) to verify the reproducibility of alternating field (AF) demagnetization performed on ~220 specimens (16 steps from 0 to 100 mT). AF demagnetization was carried out in an in-house developed robotized 2G DC SQUID magnetometer (noise level 3 × 10–12 Am^2; Mullender et al., 2016), which provides significantly better results on samples with low natural remanent magnetization (NRM) intensity.

Paleomagnetic statistical analysis was carried out using the online platform paleomagnetism.org (Koymans et al., 2016), and all data files are provided in the supporting information. Stepwise demagnetization of the NRM is displayed in orthogonal vector diagrams (Figure 4, Zijderveld, 1967). Magnetization components were determined using principle component analysis (Kirschvink, 1980) on approximately five to seven successive temperature or AF steps in the majority of the specimens. A great circle approach (McFadden & McElhinny, 1988) was used when the samples yielded directions intermediate between those of two (different) components with overlapping temperature or coercivity spectra (Figures 4o and 4p). This method iteratively determines the direction in the plane (great circle) that lies closest to the mean direction of well-determined NRM directions (set points) and the iterated great circle solutions.

Site mean directions and their statistical properties were calculated from the ChRM directions (Figure 5). A fixed cutoff (45°) was applied on the virtual geomagnetic pole (VGP) distribution, and corresponding directions were rejected. The error in declination (ΔDx) and inclination (ΔIx) were calculated separately from A95 (the 95% cone of confidence of VGPs) following Butler (1992). We derive *N*-dependent minimum and maximum values of A95 according to Deenen et al. (2011, 2014). We prefer this approach, since it provides a value of A95 that is then compared to expected values for sufficient sampling of paleosecular variation (PSV), that is, A95 must be within the range A95min–A95max.

The directions of the accepted sites are then grouped into localities that has then a mean based on the actual data (all individual directions) rather than on an average of site means. Since there are no major differences in the number of samples per site, single sites do not bias the final average. Nevertheless, for comparison, we have added locality means based on site means to Table 1. This provides very similar, final results (i.e., the amount of rotation) but different and flawed statistical parameters.

To assess whether two distributions share a common distribution, we use the nonparametric coordinate bootstrap method developed by Tauxe (2010), which uses the actual data. To test the primary origin of the ChRM, fold tests (following Tauxe & Watson, 1994) were performed on the regional data sets within a general area and age window.

4. Paleomagnetic Results

Thermomagnetic curves obtained by Curie Balance measurements are shown in Figure 3. The heating curves of most samples (Figure 3a–3d and 3l) have highest unblocking temperatures ranging 530–580 °C pointing to the presence of (Ti-poor) magnetite. Often, samples show the presence of pyrite (Figures 3e, 3f, 3i, and 3k) that transforms to magnetite above 400 °C (Passier et al., 2001). The newly formed magnetite is subsequently demagnetized/oxidized above 500 °C. In thermal demagnetization experiments, the newly formed magnetite creates spurious NRM directions. Occasionally, samples (Figures 3g, 3j, and 3h) show that the magnetization is very weak and the curves show only the paramagnetic contribution. In these samples, the Curie temperature is not clear.

Table 1
Table Showing All Paleomagnetic Data From This Study

						Chrm directions-in situ										Chrm directions-tilt corrected						
	Lat	Long	N	N_d	N_{45}	D	I	ΔDx	ΔIx	k	α_{95}	κ	$A_{95min} < A_{95} < A_{95max}$	Strike/dip	N_{45}	D	I	ΔDx	ΔIx	k	α_{95}	κ
Beyşehir basin (BB)																						
Pliocene																						
BE1	37.7080	31.7428	13	13	13	7.1	61.6	9.9	6.1	61.6	5.3	33.3	4.3 < 7.3 < 16.3	000/00	13	7.1	61.6	9.9	6.1	61.6	5.3	33.3
BE2 (spot reading)	37.9178	31.5910	14	14	14	345.5	51.8	3.2	2.9	269.9	2.4	215.8	**2.7** < A95min (4.2)	000/00	14	345.5	51.8	3.2	2.9	269.9	2.4	215.8
BE3	37.8992	31.5519	9	5	5	332.1	41.4	13.7	16.8	37.4	12.7	38.5	6.3 < 12.5 < 29.7	000/00	5	332.1	41.4	13.7	16.8	37.4	12.7	38.5
YL1	37.7575	31.6816	9	6	6	352.6	59.4	12.3	8.3	99.7	6.7	51.9	5.9 < 9.4 < 26.5	000/00	6	352.6	59.4	12.3	8.3	99.7	6.7	51.9
YA2	38.1827	31.2767	16	13	13	158.3	−64.6	11.2	6.0	58.7	5.5	29.9	4.3 < 7.7 < 16.3	245/24	13	158.8	−40.6	6.3	7.8	58.7	5.5	53.0
Late Miocene																						
Erenlerdag Volc.[1,2] (*N*)	37.5000	32.1000	8	8	8	2.4	50.2	14.9	14.2	12.2	16.5	20.0	5.2 < 12.7 < 22.1	000/00	8	2.4	50.2	14.9	14.2	12.2	16.5	20.0
Erenlerdag Volc.[1,2] (*R*)	37.5000	32.1000	10	10	10	172.5	−46.8	18.0	19.0	14.3	13.2	10.3	4.8 < 15.8 < 19.2	000/00	10	172.5	−46.8	18.0	19.0	14.3	13.2	10.3
Erenlerdag Volc.[1,2] (*N* + *R*)	37.5000	32.1000	18	18	16	1.7	46.1	8.5	9.2	18.3	8.9	25.0	4.0 < 7.5 < 14.3	000/00	16	1.7	46.1	8.5	9.2	18.3	8.9	25.0
Mean (*N*)			39	32	32	356.1	56.0	7.4	5.8	21.3	5.6	19.2	3.0 < 6.0 < 9.2		32	356.1	56.0	7.4	5.8	21.3	5.6	19.2
Mean (*R*)			26	23	23	166.0	−57.3	10.8	8.0	19.2	7.1	13.6	3.4 < 8.5 < 11.4		23	164.3	−43.4	8.2	9.6	23.3	6.4	17.7
Mean (*N* + *R*)			65	55	55	352.0	56.6	6.3	4.8	20.3	4.4	15.7	2.4 < 5.0 < 6.6		55	350.4	50.9	5.8	5.4	19.1	4.5	16.0
Mean (site avs.)			6	5	5	349.7	55.4	18.7	14.8	36.3	12.9	26.9	6.3 < 15.0 < 29.7		5	348.6	50.6	17.7	16.6	34.6	13.2	26.8
Yalvaç basin (YB)																						
Middle Miocene																						
YA3	38.3863	31.1373				No interpretable results								047/36		No interpretable results						
YA4	38.3961	31.1222	15	15	15	32.3	40.8	5.8	7.3	50.8	5.4	52.1	4.1 < 5.3 < 14.9	092/18	15	43.0	56.3	8.5	6.5	50.8	5.4	32.6
YA5 (PDF)	38.4145	31.1060	21	13	13	352.5	46.6	5.9	6.3	66.0	5.1	63.5	4.3 < 5.2 < 16.3	008/11	13	4.5	48.4	6.4	6.5	66.0	5.1	56.5
YA6	38.4495	31.0801	18	16	16	196.3	−35.5	6.7	9.4	37.6	6.1	35.0	4.0 < 6.3 < 14.3	044/32	16	223.5	−46.3	8.2	8.8	37.6	6.1	26.8
YL2 (spot reading)	38.3922	31.1226	18	16	16	206.0	−36.1	2.2	3.0	329.5	2.0	322.1	**2.1** < A95min (4.0)	053/37	16	239.0	−46.4	2.4	2.6	329.5	2.0	292.1
YL3	38.4136	31.1054	11	11	11	229.5	−32.3	5.3	7.9	96.9	4.7	83.1	4.6 < 5.0 < 18.1	078/12	11	236.9	−38.2	5.5	7.3	96.9	4.7	80.6
YL4	38.4569	31.0612	19	15	15	207.8	−26.3	6.7	11.2	30.5	7.0	35.1	4.1 < 6.5 < 14.9	075/31	15	225.5	−48.0	8.9	9.2	30.5	7.0	24.9
YL5	38.4670	31.0402	16	16	16	241.3	−52.1	4.1	3.7	125.7	3.3	115.8	3.4 < A95min (4.0)	197/28	16	198.7	−61.8	5.9	3.6	125.7	3.3	73.9
Mean (N)			15	15	15	32.3	40.8	5.8	7.3	50.8	5.4	52.1	4.1 < 5.3 < 14.9		15	43.0	56.3	8.5	6.5	50.8	5.4	32.6
Mean (R)			64	58	58	216.2	−38.5	5.4	7.2	16.0	4.8	14.6	2.4 < 5.1 < 6.4		58	222.2	−50.2	5.2	5.0	25.0	3.8	18.4
Mean (N + R)			79	73	73	35.4	39.0	4.5	5.8	18.7	3.9	17.1	2.2 < 4.1 < 5.5		73	42.3	51.5	4.5	4.1	27.4	3.2	20.1
Mean (site avs.)			8	5	5	36.1	38.4	18.5	24.4	23.7	16.0	20.8	6.3 < 17.2 < 29.7		5	43.5	50.7	15.9	14.9	43.2	11.8	32.9
Ilgın basin (IB)																						
Middle Miocene																						
IL3	38.1521	31.8157	12	11	11	159.0	−49.0	10.0	9.9	30.8	8.4	28.9	4.6 < 8.6 < 18.1	060/06	11	159.6	−55.0	11.7	9.4	30.8	8.4	24.2
AC1	38.0297	31.9155	14	11	11	315.2	33.9	7.7	11.1	36.2	7.7	40.6	4.6 < 7.3 < 18.1	260/08	11	318.1	27.6	7.0	11.3	36.2	7.7	46.7
IL2	38.1864	31.8472	14	12	12	355.3	47.7	8.0	8.3	52.9	6.9	39.2	4.4 < 7.0 < 17.1	140/14	12	339.8	54.3	9.4	7.8	52.9	6.0	32.5
IL4 (PDF)	38.1753	31.8368	18	11	11	0.1	51.4	12.4	11.4	26.4	9.1	19.9	4.6 < 10.5 < 18.1	095/21	11	354.8	72.3	26.9	9.0	26.4	9.1	11.5
IG1	38.0805	31.8832	18	12	12	347.4	51.0	10.8	10.1	25.8	8.7	23.2	4.4 < 9.2 < 17.1	152/10	12	334.8	52.6	11.3	9.9	25.8	8.7	22.2
IG2	38.0806	31.8815	18	14	14	182.4	−48.8	5.8	5.8	71.8	4.7	62.8	4.2 < 5.1 < 15.6	154/25	14	150.7	−54.5	6.7	5.5	71.8	4.7	53.7
IG3 (spot reading)	38.0807	31.8806	17	17	17	10.0	63.4	3.4	1.9	425.1	1.7	219.8	**2.4** < A95min (3.9)	205/16	17	345.4	55.8	2.6	2.0	425.1	1.7	302.2
IG4	38.0807	31.8798	17	17	17	359.1	56.6	5.2	3.9	144.4	3.0	75.7	3.9 < 4.1 < 13.8	153/10	17	343.7	59.8	5.4	3.6	144.4	3.0	76.5
IG5	38.0424	31.8729	17	14	14	342.3	48.1	8.5	8.6	38.3	6.5	30.0	4.2 < 7.4 < 15.6	282/12	14	347.4	37.4	6.8	9.1	38.3	6.3	40.7
IG6	38.0496	31.8386	14	9	9	340.5	41.6	9.4	11.5	47.2	7.6	36.6	5.0 < 8.6 < 20.5	160/06	9	335.3	40.9	9.5	11.8	47.2	7.6	36.0
IG7	38.1118	31.7361				No Interpretable Results								102/25		No Interpretable Results						
Mean (*N*)			70	64	64	349.4	50.2	3.9	3.8	37.3	2.9	28.8	2.3 < 3.4 < 6.0		64	341.1	50.0	4.0	3.9	30.3	3.3	27.3
Mean (*R*)			30	25	25	172.3	−49.5	6.7	6.6	33.3	5.2	26.0	3.3 < 5.8 < 10.8		25	154.5	−54.8	6.2	5.0	45.3	4.4	34.0
Mean (*N* + *R*)			100	89	89	350.2	50.0	3.4	3.2	36.4	2.5	28.1	2.0 < 2.9 < 4.8		89	339.4	51.4	3.4	3.1	32.4	2.7	28.1
Mean (site avs.)			12	7	7	349.0	49.3	7.9	7.7	113.0	5.7	79.6	5.5 < 6.8 < 24.1		7	338.9	50.8	7.6	7.1	81.2	6.7	88.9
Early Miocene																						
IL1	38.3800	31.8428	14	13	13	4.5	34.5	5.9	8.4	53.4	5.7	57.0	4.3 < 5.5 < 16.3	046/04	13	6.6	37.3	6.1	8.2	53.4	5.7	54.5
AC2 (RM)	38.0765	31.8300	15	15	15	180.1	−56.9	6.1	4.6	95.4	3.9	63.6	4.1 < 4.8 < 14.9	285/31	15	187.7	−27.0	3.3	5.5	95.4	3.9	141.1

Table 1 *(continued)*

	Lat	Long	N	N_d	N_{45}	Chrm directions-in situ D	I	ΔDx	ΔIx	k	α_{95}	κ	$A_{95min} < A_{95} < A_{95max}$	Strike/dip	Chrm directions-tilt corrected N_{45}	D	I	ΔDx	ΔIx	k	α_{95}	κ
Harami[3] (*N*)	38.4500	31.8700	45	45	44	2.6	36.2	3.9	5.3	30.5	4.0	36.2	2.6 < 3.6 < 7.6	000/00	44	2.6	36.2	3.9	5.3	30.5	4.0	36.2
Harami[3] (*R*)	38.4500	31.8700	37	37	36	191.3	−40.5	5.3	6.7	23.2	5.1	24.7	2.9 < 4.9 < 8.6	000/00	36	191.3	−40.5	5.3	6.7	23.2	5.1	24.7
Mean (*N*)			59	58	57	3.1	35.9	3.2	4.5	34.1	3.3	39.9	2.4 < 3.0 < 6.4		57	3.5	36.5	3.2	4.5	33.9	3.3	39.4
Mean (*R*)			37	37	36	191.3	−40.5	5.3	6.7	23.2	5.1	24.7	2.9 < 4.9 < 8.6		36	191.3	−40.5	5.3	6.7	23.2	5.1	24.7
Mean (*N* + *R*)			96	95	94	5.7	37.9	3.0	4.0	26.2	2.9	27.8	1.9 < 2.8 < 4.7		94	6.0	38.3	3.0	4.0	26.4	2.9	27.9
Mean (site avs.)			3	2	2	5.2	36.5	6.9	9.5	797.0	8.9	1498.0	9.1 < 6.5 < 53.0		2	6.3	37.9	2.4	3.1	8664.8	2.7	12960.9
Altınapa basin (AB) - Miocene																						
Upper AB - M. Miocene																						
AP10	37.9250	32.2430	12	12	12	186.5	−63.4	12.2	6.9	47.5	6.4	26.4	4.4 < 8.6 < 17.1	190/30	12	146.0	−48.0	8.1	8.2	47.5	7.0	39.0
UM1	37.9297	32.2254	18	15	15	351.1	50.8	6.4	6.0	65.2	4.8	50.3	4.1 < 5.4 < 14.9	160/21	15	326.0	48.6	6.3	6.3	65.2	4.8	50.1
UM2	37.9266	32.2415		6	6	9.0	51.5	12.0	11.0	54.4	9.2	44.5	5.9 < 10.1 < 26.5	190/30	6	338.9	40.4	9.3	11.7	54.4	9.2	62.8
BR1 (PTM)	37.9902	32.2284	14	12	12	158.0	−55.8	13.3	10.4	19.8	10.0	17.4	4.4 < 10.7 < 17.1	306/34	12	184.2	−32.7	9.8	14.5	19.8	10.0	22.7
BR2 (PDF)	38.0482	32.2876	14	12	12	358.0	55.4	6.1	4.9	98.4	4.4	77.9	4.4 < 4.9 < 17.1	037/38	12	67.2	62.8	8.3	4.8	98.4	4.4	54.1
BR3 (PDF)	38.0284	32.2515	15	14	14	358.9	55.9	7.6	5.9	76.2	4.6	43.4	4.2 < 6.1 < 15.6	094/36	14	255.5	84.1	46.4	4.3	76.2	4.6	23.6
BR4 (PTM)	38.0034	32.2091	11	11	11	138.1	−46.2	14.5	15.6	18.7	10.8	13.6	4.6 < 12.8 < 18.1	185/31	11	126.8	−19.8	8.9	16.0	18.7	10.8	28.1
BR5 (PTM)	38.0313	32.1695	13	5	5	172.4	−58.6	17.6	12.3	40.7	12.1	32.8	6.3 < 13.6 < 29.7	105/16	5	151.0	−71.5	32.4	11.3	40.7	12.1	20.4
Sille volcanics[1]	37.9000	32.4000	5	5	5	155.2	−53.1	17.2	14.8	45.5	11.5	29.8	6.3 < 14.3 < 29.7	000/00	5	155.2	−53.1	17.2	14.8	45.5	11.5	29.8
Mean (*N*)				21	21	356.1	51.3	6.2	5.8	51.7	4.5	37.0	3.6 < 5.3 < 12		21	330.1	46.4	5.6	6.0	49.6	4.6	42.6
Mean (*R*)			55	45	43	162.4	−57.3	7.4	5.5	22.1	4.7	14.9	2.7 < 5.8 < 7.7		45	150.2	−51.8	6.3	5.7	22.9	4.5	17.1
Mean (*N* + *R*)				66	64	347.5	55.4	5.4	4.3	25.2	3.6	17.2	2.3 < 4.4 < 6		66	330.2	50.1	4.6	4.4	27.2	3.4	20.9
Mean (site avs.)			9	7	7	346.0	55.4	14.9	11.8	45.2	9.1	26.1	5.5 < 12 < 24.1		7	332.8	50.5	9.6	9.1	75.8	7.0	54.8
Lower AB - E.Miocene																						
AP1	37.8977	32.3018	14	12	12	354.8	60.3	13.6	8.8	36.3	7.3	19.2	4.4 < 10.2 < 17.1	280/12	12	359.8	48.8	9.9	9.8	36.3	7.3	26.7
AP2	37.8977	32.3013	14	14	14	15.4	70.0	13.0	5.1	65.5	4.9	28.2	4.2 < 7.6 < 15.6	246/11	14	357.9	49.1	6.5	6.5	65.5	4.9	50.5
AP3 (PDF)	37.8986	32.2920	13	13	13	359.9	51.6	10.4	9.5	31.0	7.6	23.2	4.3 < 8.8 < 16.3	272/22	13	1.8	29.7	6.7	10.5	31.0	7.6	42.8
AP4	37.9347	32.3007	25	25	25	183.2	−29.1	4.3	6.9	44.6	4.4	49.2	3.3 < 4.2 < 10.83	118/14	25	178.0	−41.0	5.1	6.4	44.6	4.4	38.7
AP5	37.9345	32.2995	22	22	22	191.7	−26.8	5.1	8.4	36.7	5.2	40.1	3.5 < 5.0 < 11.7	127/29	22	177.4	−50.3	7.5	7.1	36.7	5.2	24.2
AP6	37.9342	32.2992	19	19	19	173.6	−35.7	4.3	6.0	82.3	3.7	70.5	3.7 < 4.0 < 12.8	093/14	19	170.2	−49.2	5.4	5.3	82.3	3.7	52.4
AP7 (spot reading)	37.9337	32.2988	16	16	16	178.9	−34.9	2.6	3.6	171.8	2.8	211.5	2.4 < A95min (4.0)	112/24	16	165.2	−54.9	4.0	3.3	171.8	2.8	126.9
AP8	37.9311	32.2985	13	10	10	192.5	−38.5	11.5	15.2	25.8	9.7	21.4	4.8 < 10.7 < 19.2	168/20	10	175.5	−42.5	12.4	14.8	25.8	9.7	19.4
AP9 (spot reading)	37.9303	32.2984	14	14	14	180.8	−32.8	3.5	5.2	72.5	4.7	143.7	**3.3** < A95min (4.2)	168/20	14	167.6	−33.4	3.5	5.1	72.5	4.7	146.8
Mean (*N*)			28	26	26	4.1	65.9	10.1	5.0	37.8	4.7	18.7	3.3 < 6.7 < 10.5		26	358.8	49.0	5.4	5.4	49.7	4.1	37.1
Mean (*R*)			79	76	76	184.6	−31.0	3.0	4.6	32.3	2.9	32.4	2.1 < 2.9 < 5.4		76	175.6	−46.0	3.4	3.7	38.8	2.6	29.7
Mean (*N* + *R*)			107	102	101	4.5	39.7	3.9	5.0	16.5	3.6	16.3	1.9 < 3.6 < 4.5		102	356.4	46.8	2.9	3.1	40.9	2.2	31.2
Mean (site avs.)			9	6	6	4.9	43.6	16.9	19.6	18.8	15.8	20.4	5.9 < 15.2 < 26.5		6	356.5	46.9	4.1	4.3	312.9	3.8	343.5

Note. Lat = latitude of the sites; Long = longitude of the site; *N* = number of measured samples; Nd = number samples after interpretation; N45 = number of samples application of a fixed cutoff (45°); *D* = declination; *I* = inclination; ΔDx = declination error; ΔIx = inclination error; *k* = estimate of the precision parameter determined from the ChRM directions; α95 = cone of confidence determined from the ChRM directions; *K* = precision parameter determined from the mean virtual geomagnetic pole (VGP) direction; A95 = cone of confidence determined from the mean VGP direction. A95min and A95max correspond to the confidence envelope of Deenen et al. (2011). If A95 falls within this envelope the distribution likely represents paleosecular variation. If A95 < A95min the distribution is too tight and represents a spot reading of the field. All values are given before and after correction for bedding tilt. Strike/dip, bedding planes for the samples included in the calculation of the ChRM directions. PTM = post-tilt magnetization; RM = remagnetization; PDF = present-day magnetic field; Mean (site avs.) = locality mean calculated from site averages. 1 = data from Tatar et al. (2002); 2 = data from Platzman et al. (1998); 3 = data from Krijgsman et al. (1996).

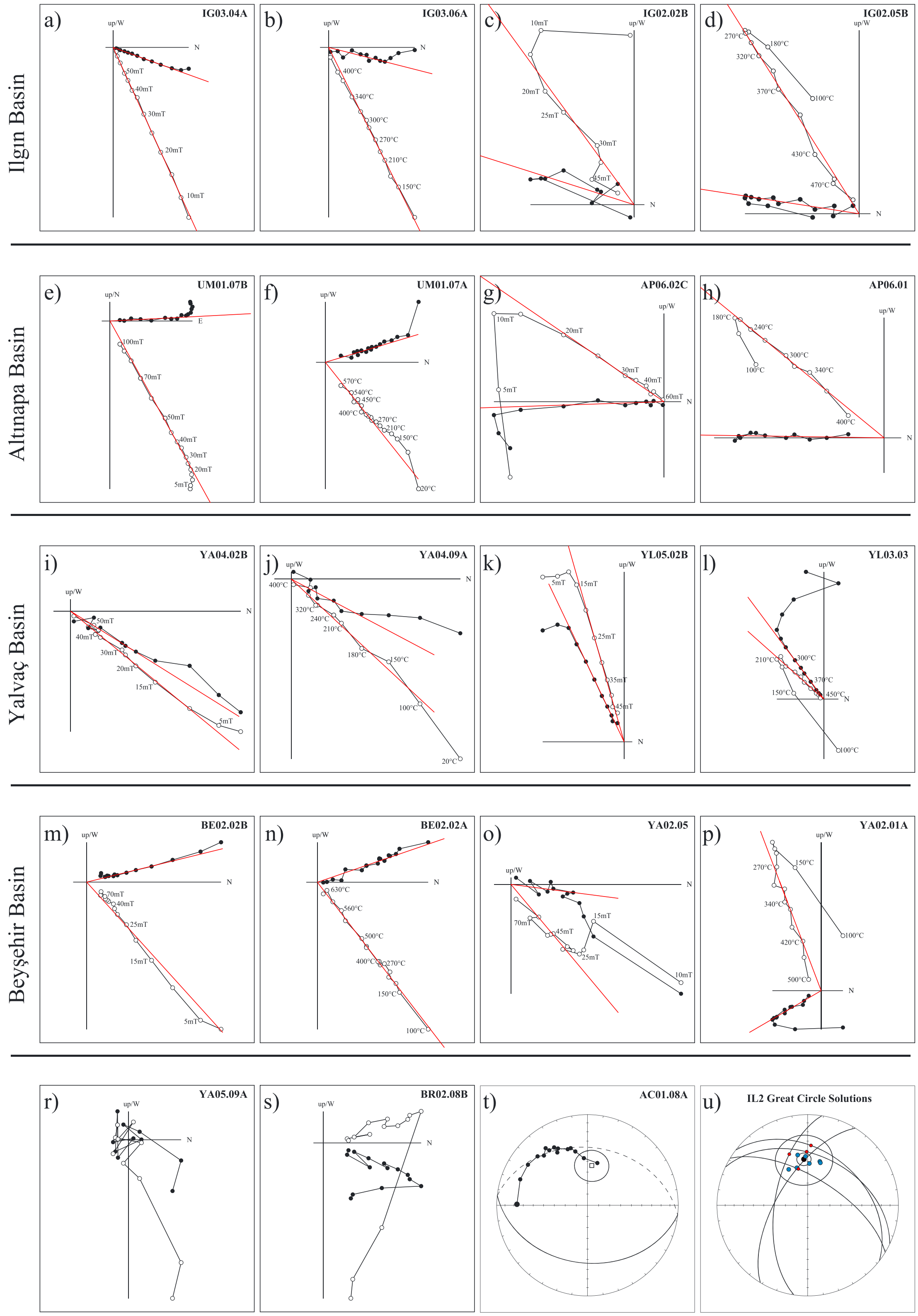

Figure 4. Orthogonal vector diagrams (Zijderveld, 1967) showing representative demagnetization diagrams for all basins. Closed (open) circles indicate projection on the horizontal (vertical) plane. All diagrams are in a geographic reference frame. For several samples, both alternating field (steps in milli Tesla) and thermal (steps in degree Celsius) demagnetization diagrams are given to show their similarity. For some sites, we used great circles and calculated great circle solutions according to McFadden and McElhinny (1988).

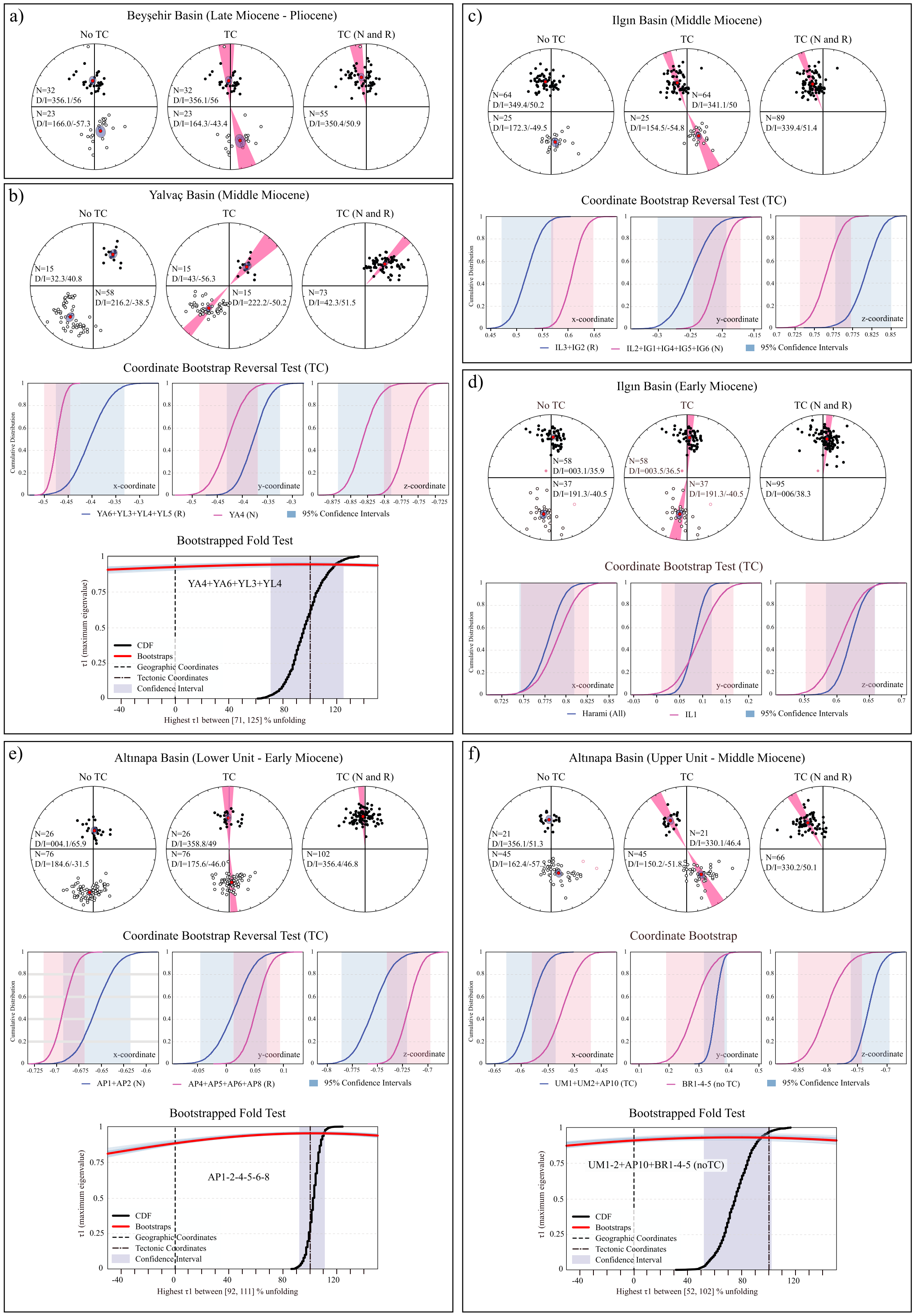

Figure 5. Equal area projection of the ChRM directions for the (a) Beysehir, (b) Yalvaç, (c, d) Ilgın, and (e, f) Altınapa basins. Closed (open) symbols indicate projection on lower (upper) hemisphere. Large red circles with blue transparent ellipse denote, respectively, the mean directions and the (ΔDx, ΔIx) ellipse. For all basins except Beysehir the final normal and reversed distributions share a common distribution following the bootstrap coordinate test (Tauxe, 2010). In addition, the results from the Yalvaç and Altınapa show positive fold tests.

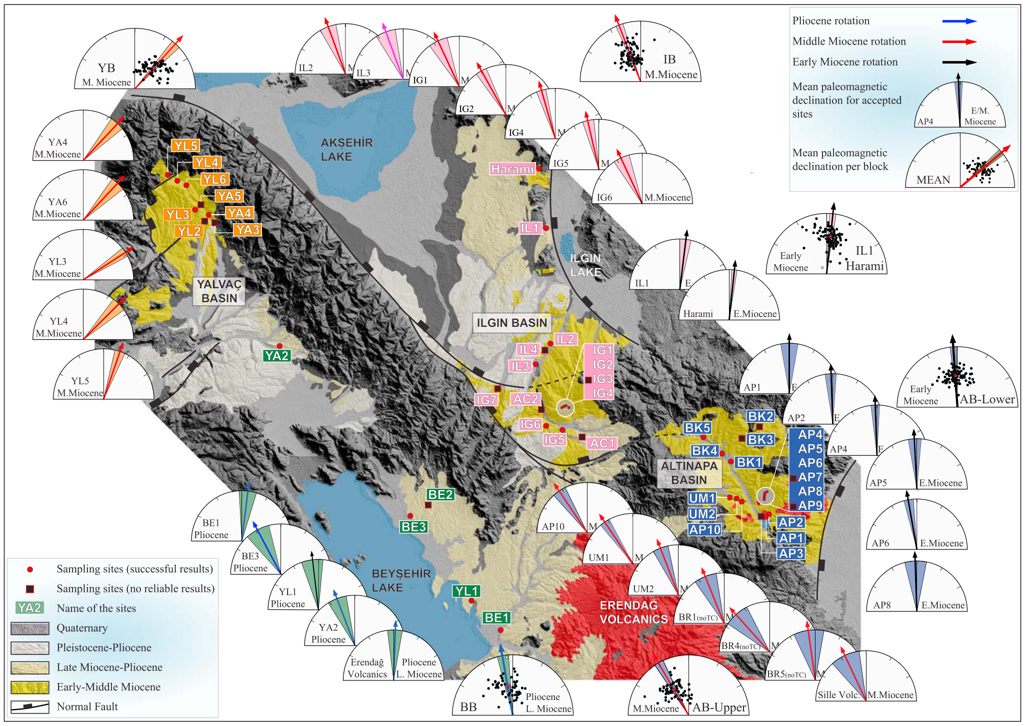

Figure 6. Map showing the locations of the sites and their declinations (arrows) with their corresponding ΔDx (colored shading). The same shading color indicates sites from the same basin or unit (lower and upper Altınapa units), the color of the arrow refers to the age of the sites: Early Miocene (black), Middle Miocene (red), and Late Miocene to Pliocene (blue). The mean per basin or unit is given in the larger equal area projections together with all used individual directions (dots). We also include the results from Harami (Krijgsman et al., 1996).

Equal area projections of the mean ChRM directions of all sites are displayed in Figure 5. Details per locality are given in Figure 6 and Table 1. In many samples, a small viscous component is removed at low temperatures (100 °C) or at low AFs (~10 mT). A secondary component with a recent direction—close to the geocentric axial dipole (GAD) field for the locality—is generally removed at temperatures around 200–240 °C (Figure 4). Thermal demagnetization analysis supports that in many cases the principal magnetic carrier of the ChRM in samples is carried by (Ti-poor) magnetite (530–580 °C), in line with the Curie balance results. If transformation of pyrite to magnetite occurs, the results above 400 °C are often obscured in the thermal demagnetizations.

In our analysis of the four basins below, we include previously published paleomagnetic results. Tatar et al. (2002) reported paleomagnetic data from 5 lavas of the Middle Miocene (~11.8 Ma) Sille volcanics in the east of the IB and 18 lava sites from the Miocene (~8–12 Ma) Erenlerdağ volcanics in the southeast of the BB. Platzman et al. (1998) added another three lava sites from the Erenlerdağ volcanics. Using the criterion that lava sites must have $k > 50$ (Biggin et al., 2008), we accepted the 5 sites for the Sille volcanics plus $16 + 2 = 18$ volcanic sites to represent the Erendağ volcanics. Finally, we used the original data for the Early Miocene (~23–21.5 Ma) Harami section in the IB reported by Krijgsman et al. (1996).

4.1. Beyşehir Basin

We collected five sites from Pliocene sediments of BB (Table 1; Figure 5a), of which four (BE1, BE2, BE3, and YL1) have normal and one (YA2) has reversed polarity. The sites gave well-defined components decaying toward the origin, both with AF and thermal demagnetization. Site BE2 yields a very tight clustering with A95 = 2.7° < A95min = 4.2°, however, and hence does not represent PSV (spot reading of the field or remagnetization); this site was therefore rejected.

The single reversed site (YA2) shows a positive reversal test with one of the normal sites (BE3) but not with the other two normal sites (BE1 and YL1). Although these latter two sites are close to the GAD field, we see no reason to exclude them from our average considering the consistent and overall good quality of the demagnetization results. We then combine our new results (N = 37) with previously reported data (N = 18) from the Upper Miocene to the Pliocene Erenlerdağ volcanics (Platzman et al., 1998; Tatar et al., 2002), showing that the BB underwent a CCW vertical axis rotation of 9.6 ± 5.8° since the Late Mio-Pliocene.

4.2. Yalvaç Basin

We collected eight sites from Middle Miocene fluvio-lacustrine clastic sediments and marls in the YB, two normal (YA4 and YA5), five reversed (YA6, YL2, YL3, YL4, and YL5), and one (YA3) that did not yield any interpretable results (Table 1 and Figure 5b). Site YA5 yielded normal directions that before and after tilt correction are close to the recent GAD field, and we suspect recent remagnetization; this site was rejected. Site YL2 yields a very tight clustering with A95 $<$ A95min, both in geographic and tectonic coordinates, and therefore cannot represent PSV; this site was also rejected. Site YL5 shows a tight clustering in geographic coordinates but passes the A95 criterion in tectonic coordinates and hence was accepted.

The accepted five Miocene sites show both normal (1) and reversed (4) polarities (Table 1). Normal polarity site YA4 gives demagnetization behavior with a well-defined component decaying toward the origin, a data scatter within the range expected from PSV, and a rotated component with the expected inclination for the Miocene paleolatitude of Turkey (Table 1). These criteria support a primary magnetization. The four reversed sites (YA6, YL3, YL4, and YL5) also provide well-defined magnetization components that trend toward the origin of the demagnetization diagrams. The middle Miocene sites of the YB yield a positive reversal test (Figure 5b), while the fold test is also positive provided we do not include YL5 (Figure 5b). The mean of the five sites (N = 73) shows a robust and large CW vertical rotation of 42.3 ± 4.5° since the Middle Miocene.

4.3. Ilgın Basin

In the IB, from a total of 13 sites, 11 were collected from Middle Miocene sediments and 2 from Early Miocene sediments. From the two Early Miocene sites, we rejected one site (AC2): it has reversed polarity, but the in situ mean inclination (I = −56.9°) of the site corresponds to the recent magnetic field, whereas after tilt correction the inclination of the site is abnormally shallow (I = −27.0°), which would require unrealistically high compaction. We suspect this site to be remagnetized during a recent reversed interval, consistent with A95 = 3.2° $<$ A95min = 4.1° (Table 1). We accept the other site from Lower Miocene sediments (IL1), which has a negligible net rotation (6.6 ± 6.1° CW). This is in excellent agreement with the large data set (N = 82) of the Harami section (Krijgsman et al., 1996; Figure 5d) that revealed an identical direction (5.9 ± 3.4° CW), as shown by the Cartesian bootstrap test (Figure 5d). The combined Harami + IL1 results then gives a small net rotation (6.0 ± 3.0° CW).

From the 11 Middle Miocene sites, we discard 4 sites. Site AC1 has an anomalously low inclination in geographic coordinates (I = 33.9°) that even becomes shallower after tilt correction (I = 27.6°). The mean direction in geographic coordinates of site IL4 coincides with the recent magnetic field, whereas in tectonic coordinates, the inclination of the IL4 is too steep (I = 72.3°). We interpret this site as representing a recent magnetic field overprint, and hence, we reject this site. Since demagnetization diagrams from site IG7 did not yield interpretable ChRM directions we had to discard this site. Finally, site IG3 yields a very tight clustering with A95 $<$ A95min, pointing to a spot reading of the field and was rejected.

The remaining seven sites are of normal (IL2, IG1, IG4, IG5, and IG6) and reversed (IL3 and IG2) polarity Figure 5c) that all pass the Deenen et al. (2011) criteria (Table 1). The combined normal and combined reversed directions pass the reversal test (Figure 5c) but not the fold test. The combined mean direction provides clear evidence that the IB underwent a net CCW rotation of 20.6 ± 3.4° since the Middle-Late Miocene.

4.4. Altınapa Basin

The Altınapa basin (AB) has 17 sites, divided in two groups/units that are constrained by their age: 9 sites from the Early Miocene lower Altınapa unit and 8 sites from the Middle Miocene upper Altınapa unit (Koç et al., 2012; Table 1 and Figure 5e).

From the lower Altınapa unit (Figure 5e) we discarded three sites: Site AP3 because it is a recent field overprint as evidenced by its pretilt direction (D/I = 360°/52°) and its too low inclination (I = 30) after tilt correction; sites AP7 and AP9 have A95 values below A95min and must be regarded as spot readings of the field or caused by remagnetization. The other six sites gave both normal (AP1 and AP2) and reversed (AP4, AP5, AP6, and AP8) polarities that provide a positive reversal test (Figure 5e). The fold test applied to all sites

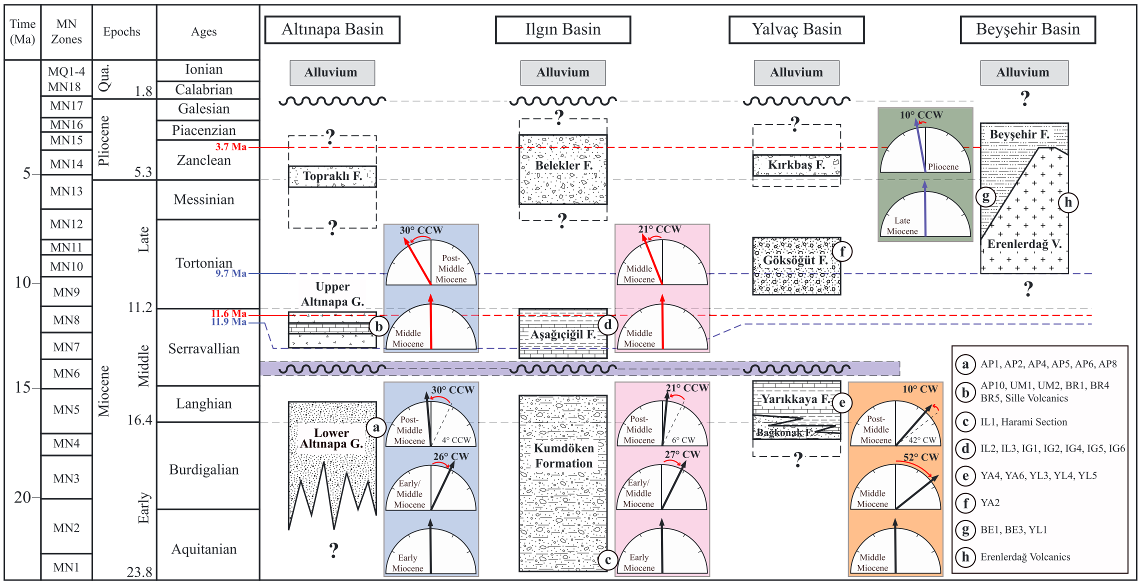

Figure 7. Correlation of the unconformity bounded lithological units of each basin. The main angular unconformity surface occurred during the Middle Miocene (~12 Ma). The rotational history is given in the stratigraphy below and above the unconformity surface. Letters a–h along the lithological columns indicate the position of the paleomagnetic sites given in the legend.

provides a tight cluster around 100% unfolding (Figure 5e). The good and consistent results together (N = 102) document a negligible rotation of 3.6 ± 2.9° CCW after tilt correction. The mean inclination (46.8 ± 3.1°) is within very reasonable values if we take sedimentary compaction into account.

From the upper Altınapa unit (Figure 5f) we discarded two sites (BR2 and BR3) because of a clearly recent overprint before tilt correction (on average D/I = 359°/56°) and inconsistent directions after tilt correction (Table 1). Another three sites (BR1, BR4, and BR5) display a clear post-tilt remagnetization based on anomalously low (I = 20°, I = 33°) or steep (I = 72°) inclinations if we apply tilt correction (Table 1). However, their combined pretilt directions are very consistent with the combined tilt corrected directions of AP10, UM1, and UM2; the two distributions share a common distribution according to the coordinate bootstrap test (Figure 5f). In addition, both distributions also share each a common distribution with the Sille volcanics (Tatar et al., 2002), while also the combined normal ((UM1 and UM2) and combined reversed (AP10, BR1, BR4, and BR5) directions share a common distribution. The fold test on our new directions (N = 61) shows a 95% interval of [52–102%] unfolding for maximum eigenvalues, so it just includes a positive fold test (Figure 5f). Hence, we joined all directions (N = 61) together with the Sille volcanics (N = 5) to a single distribution for the Altınapa lower unit (N = 66) that shows a considerable CCW rotation of 29.8 ± 4.6°.

5. Discussion

Our new paleomagnetic results of the CTIB reveal that the four studied basins show rotations that differ in space and time (Figures 6 and 7). Together with previously published paleomagnetic data from the Bey Dağları, Aksu, Köprüçay, Manavgat, and Afyon regions from Middle Miocene to Pliocene rocks (Gürsoy et al., 2003; Kissel & Poisson, 1986, 1987; Koç, van Hinsbergen, et al., 2016; Morris & Robertson, 1993; Tatar et al., 2002; van Hinsbergen, Dekkers, & Koç, 2010), we may now attempt a first-order map-view restoration of the kinematic evolution of the region since the early Miocene.

Koç, Kaymakci, et al. (2016) suggested that the Central Tauride orocline represents essentially intraplate deformation, whereby the oroclinal bending is accommodated by the opposite rotation of two limbs of the orocline (Figure 8) that end in pivot points where they connect to a more or less stable Central Anatolia. If this is correct, this would require an increasing amount of ~E-W extension from the pivots to the center of the orocline. The motions of fault blocks along major normal faults in the region (Koç et al., 2017, 2012; Koç, van Hinsbergen, et al., 2016) accommodate rotations as constrained in this paper; hence,

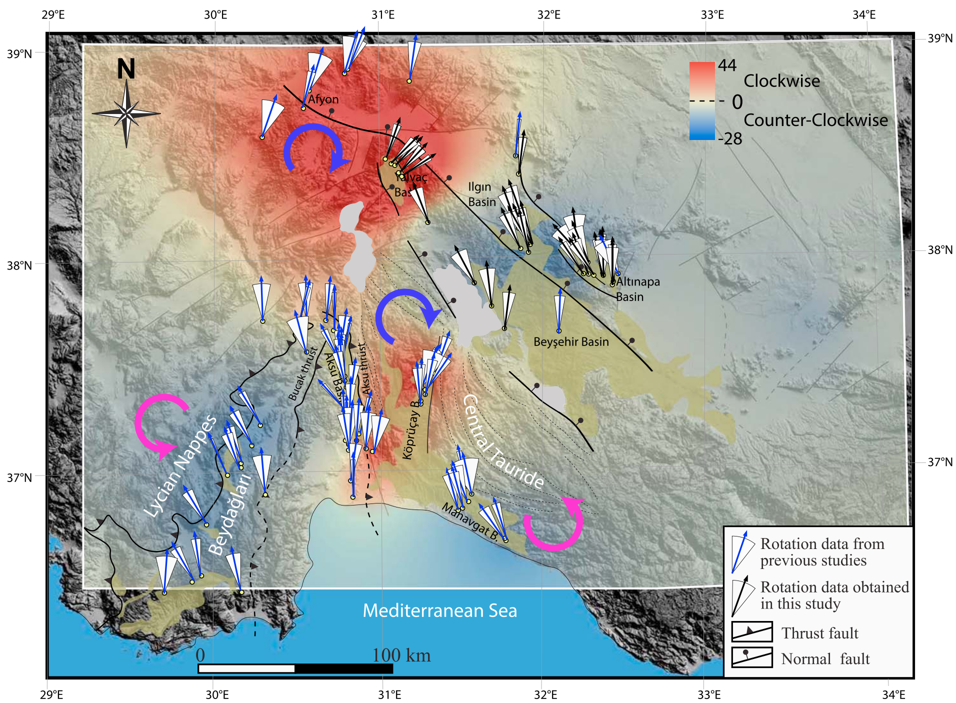

Figure 8. Interpolated regional distribution of declination of mean paleomagnetic vectors with cones of 95% confidence from Neogene rock units adjusted for tectonic tilts. All directions are shown with normal polarity. Red and blue colors indicate clockwise and counterclockwise rotational domains.

the aim of our restoration is to assess whether these motions would accommodate the predicted amount of extension relative to Central Anatolia.

We treat Central Anatolia to the east of the documented major normal faults in the Konya and Ilgın regions as a rigid block since ~20 Ma. Major rotations and associated shortening occurred largely in the Oligocene to perhaps earliest Miocene (Advokaat et al., 2014; Gülyüz et al., 2013; Gürer et al., 2016, 2018; Işık et al., 2003). Some Pliocene E-W extension is accommodated to the east of the CTIB, in the Tuz Gölü basin (Fernandez-Blanco et al., 2013) and along the Ecemis fault (Higgins et al., 2015; Jaffey & Robertson, 2005), but documented displacements are small. We therefore assume that the region to the east of the CTIB did not experience major deformation in the last 20 Myr and evaluate this assumption later in the light of our discussion. To the west, the orocline is bounded by the Bey Dağları platform, which has been rotating CCW in Miocene time (Figure 8; Morris & Robertson, 1993; van Hinsbergen, Dekkers, & Koç, 2010), accommodated along the Aksu and Bucak thrusts (Koç, van Hinsbergen, et al., 2016).

We determine a pivot point of the northern limb of the orocline in the region of Afyon, where Gürsoy et al. (2003) identified ~20° CW rotation, similar to that documented by Koç, van Hinsbergen, et al., (2016) in the Köprüçay basin, accommodated since ~20 Ma (Figure 8). The southern limb of the orocline underwent a post-20 Ma, ~20° CCW rotation and thus predicts a limb size equal to the northern limb, which suggests a pivot point relative to a stable Central Anatolia in the Mut basin (Figures 9a–9c). This restoration predicts a maximum amount of post-20 Ma E-W extension around Beyşehir, of up to ~60 km.

Within the CTIB domain, we then identify several fault-bounded blocks, whereby the northern half of the extensional domain to the east of the orocline is well exposed. The southern half is overlain by young volcanics, young sediments, or no sediments, and its kinematic history is therefore more challenging to reconstruct. Our analysis therefore focuses on the northern region, including the Beyşehir, Altınapa, Ilgın, and YBs. From east to west, we include the Altınapa block bounded by the Konya fault in the southeast and the Ilgın fault in the west, and an ill-defined fault in the north buried below the Tuzgölü basin. Within the Ilgın and Aksehir basins, we identify five fault bounded blocks. These are bounded from the Sultandağları footwall by the major normal faults of Aksehir-Afyon in the southwest, from the Altınapa

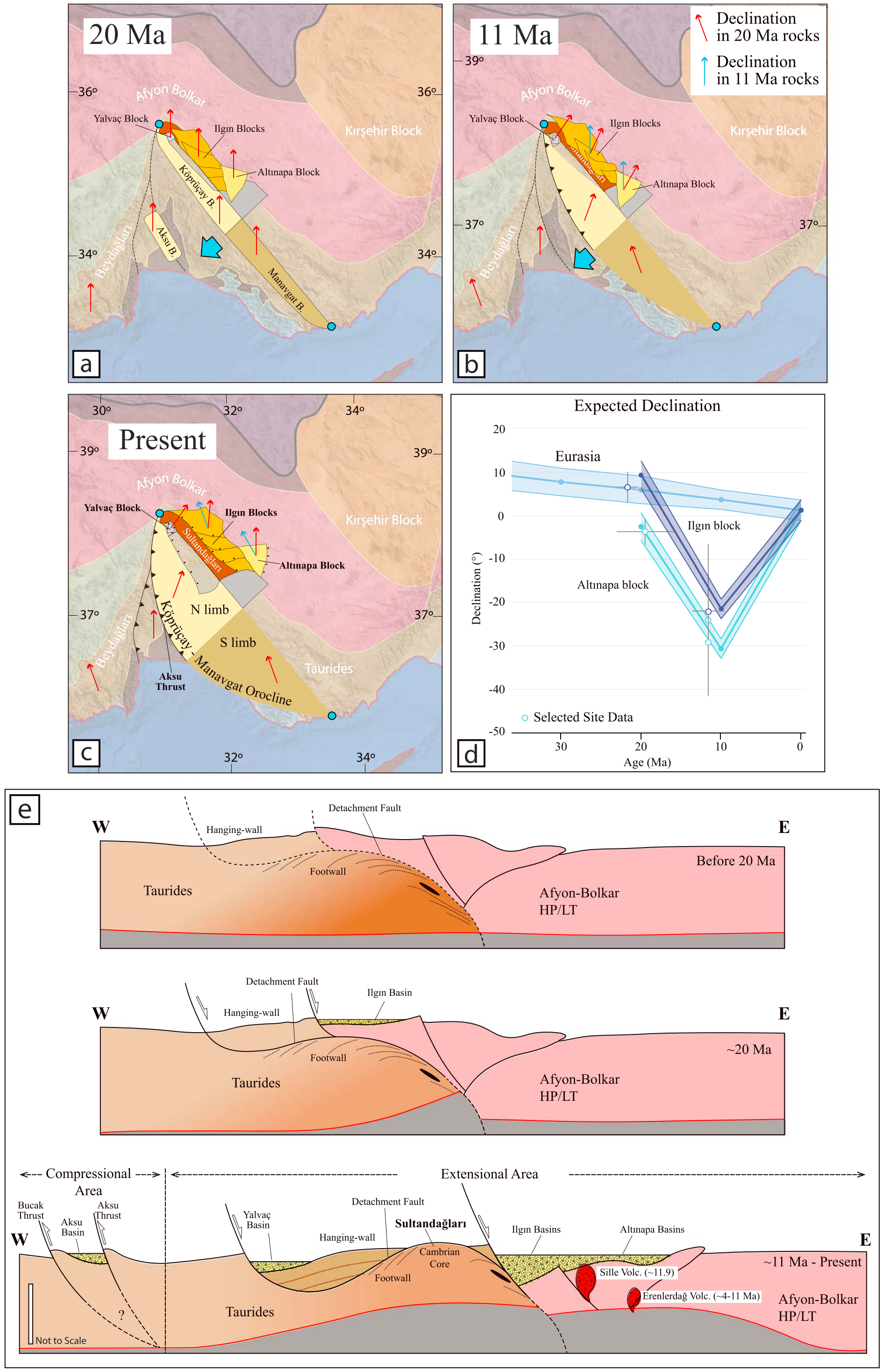

Figure 9. First-order kinematic reconstruction of the central Tauride orocline and the central Tauride intramontane basins, cast in the paleomagnetic reference frame of Torsvik et al. (2012). Reconstruction of the Anatolia versus Eurasia follows van Hinsbergen and Schmid (2012) and Gürer and van Hinsbergen (2018). For reference, we superimpose the reconstructed Taurides on the outline of the modern geography of Anatolia. We did not incorporate detailed reconstructions of Beydağları but focus on our study area in the central Taurides instead (a–c). See text for further explanation. Test of our reconstruction of fault block motion against the paleomagnetic constraints is illustrated as local Apparent Polar Wander Paths (APWPs) of the Ilgın and Altınapa basins versus the Eurasian APWP. The predicted rotations of the different blocks by our reconstruction are consistent with the measured paleomagnetic data (d). The evolutionary schematic (not to scale) cross sections illustrate the complex tectonic setting of the region with crustal scale (e).

block and stable Central Anatolia to the east by the Ilgın fault, and from each other by the E-W trending Argıthanı, Balkı, Derbent, and Kızılören faults (Figure 2). The Sultandağları massif is assumed to form a coherent block, separated from the main Tauride belt that constitutes the northern limb of the orocline by the Yalvaç-Beyşehir graben, within which the Yalvaç block forms the northernmost part. Finally, the main Beyşehir basin is modeled as a single block bounded to the east by the Aksehir-Afyon fault zone and to the west by the Beyşehir fault. To the north, the boundary with the Sultandağları block is diffuse, and the southern boundary is unconstrained due to overlying young volcanics.

Rotations of these blocks follow from our new paleomagnetic constraints. Rocks in the Ilgın and Altınapa basins reveal CCW rotations (Figures 6 and 7) for the Middle Miocene deposits (post ~12 Ma), of, respectively, ~21 ± 3° CCW (Ilgın) and ~30 ± 5° CCW (Altınapa upper unit). In both basins, we also obtained paleomagnetic data from Lower Miocene sediments, which in the Harami section of the IB was constrained at an age of ~22 Ma (Krijgsman et al., 1996). The IL1 and Harami section in the IB reveal a net rotation of only ~6 ± 3° CW. This suggests that between ~22 and ~12 Ma, the basin (s) must have undergone first a rotation of 27 ± 4° CW followed by the post-12 Ma rotation of ~21° CCW. A comparable history affected the Altınapa basin whereby the declination retrieved from the Altınapa lower unit is only 4° CW, suggesting a 26° CW Early-Middle Miocene rotation, followed by a ~30° CCW since the Middle Miocene (Figure 7).

Koç et al. (2017) documented a distinct stratigraphic break in both continental basins—expressed as an angular unconformity (Figure 7). This unconformity marks the change from clastics to lacustrine limestones (intercalating with volcanic input in Altınapa; Koç et al., 2012). The Serravallian unconformity therefore represents the onset of significant subsidence of the Ilgın and Altınapa basins. We therefore correlate this change in the sense of rotation in the Ilgın and Altınapa basins from regional CW rotation to CCW to this stratigraphic break and associated unconformity, which has an age of ~12 Ma (Koç et al., 2017, 2012; see Figure 7).

The younger YB was subjected to a net rotation (of ~42° CW) since the Middle Miocene, but older (Early Miocene) sediments are not exposed (Figure 7). This is approximately 25° more than the rotation of the northern limb of the orocline, and this additional rotation is thus likely related to a local fault block rotation. In the YB, a similar Serravallian unconformity was identified (Figure 7), but while the unconformity in the Ilgın and Altınapa basins marks the change from clastics to lacustrine limestone, in the Yalvac basin it marks the transition from lacustrine limestones to conglomeratic (boulder to block size) clastics (Koç, Kaymakci, et al., 2016). From this analysis we infer that all basins likely underwent a ~25° CW rotation between ~20 and 12 Ma, after which the Ilgın and Altınapa basins underwent CCW rotations (of 21° and 30°, respectively). Finally, from the Beyşehir basin, only Upper Miocene and Pliocene sediments and volcanics are available for paleomagnetic analysis and show ~10 ± 6° CCW rotation.

All major fault zones bounding and cutting the Yalvaç, Ilgın, and Altınapa basins are clearly extensional (Koç et al., 2017; Koç, Kaymakci, et al., 2016; Koç et al., 2012; Koçyiğit & Saraç, 2000), and the observed rotations since the late Middle Miocene must therefore be related to extensional deformation controlled by low- and/or high-angle normal faults. Our reconstruction now attempts to restore the paleomagnetically documented rotations while obeying the kinematic boundary conditions posed by the documented faults.

First we restore the IB rotations relative to the Sultandağları footwall at 12 Ma. CCW block rotation accommodated by normal faulting is modeled by assuming an Euler pole in the southwest of the rotating domain, whereby the minimum amount of extension is obtained by assuming the pole is located at the fault interface. Assuming that whole basin to the east of the Sultandağları massif rotated as a rigid block would generate an unrealistic reconstruction whereby the northern part of the basin restores west of the YB. We therefore apply a ~20° CCW rotation to each of the smaller fault blocks bounded by the E-W trending normal faults outlined in Figure 2, around poles in the southwest of the fault blocks. This generates a restored overlap between the fault blocks and the Sultandağları massif that represents post-12 Ma extensional slip. This restoration also generates small overlaps between the fault blocks along the E-W trending normal faults. We restore the double rotation history of the Altınapa block in a similar fashion, leading to overlaps along the Ilgın fault.

Restoring the 20–12 Ma ~25° CW rotation phase follows a similar approach, but the opposite sense of rotation requires shifting the Euler poles of the fault blocks relative to the Sultandağları footwall to the northwest of the blocks. Restoring the CW rotations then generates an almost complete overlap between the Sultandağları footwall and the hanging wall basin blocks of the Altınapa-IB.

Sedimentological and structural analysis of the YB has revealed that its modern margins are defined by Lower Miocene basin-bounding normal faults and has always been located between the Sultandağları massif and the main Tauride axis. To the south, we have no direct constraints on the structure and stratigraphy. We therefore restore a maximum rotation juxtaposing the western margin of the Sultandağları massif against the eastern margin of the Taurides west of the Beyşehir fault, equaling the ~15-km width of the Yalvac-Beyşehir valley. We model the large (in total 42° CW) rotation of the YB as a local rotation in excess of the regional rotation of the northern oroclinal limb, due to a lateral variation in normal slip along the four basin-bounding normal faults.

We test our restoration of fault block motions against the paleomagnetic constraints following the recent approach of Li et al. (2017; Figure 9d). To this end, we computed the Euler pole of each fault block in our reconstruction relative to South Africa, using the restoration of Anatolian extrusion relative to Eurasia of van Hinsbergen and Schmid (2012), and the Atlantic Plate Circuit summarized in Seton et al. (2012) updated with north Atlantic poles of DeMets et al. (2015). We then used paleomagnetism.org (Koymans et al., 2016) to compute the Global Apparent Polar Wander Path of Torsvik et al. (2012) in the coordinates of our fault blocks (in 10 Myr intervals) and compare these to our in situ paleomagnetic data from each fault block. All block restorations are consistent with the paleomagnetic constraints (Figure 9d). In addition, restoration of these rotations suggests that the basins accommodated simultaneous ~E-W and N-S extension, which is consistent with extensive field documentation based on small-scale growth faults that show bidirectional extension on the basin scale in all CTIB basins (Koç et al., 2017; Koç, Kaymakci, et al., 2016; Koç et al., 2012).

The restoration predicts that up to ~50–60 km of E-W extension was accommodated in the center of the Central Tauride orocline, which is fully consistent with the prediction based on restoring oroclinal bending. This may be used as an argument to confirm that the orocline formed because of a westward pull, or collapse, of the Central Taurides in Miocene time as inferred by Koç, van Hinsbergen, et al. (2016). In other words, we conclude that the CTIB extension is intrinsically related to the formation of the Central Tauride orocline, and any dynamic explanation, likely involving some role for the Antalya slab, should explain both features in tandem.

Finally, we remark that our reconstruction suggests that the Sultandağları range has been entirely exhumed from below the Altınapa-IB in Miocene time. This amounts to ~30–35 km of E-W extension accommodated along a single normal fault (zone) to which the Sultandağları range was the footwall. This predicts that the Sultandağları range, which exposes low-grade metamorphic Paleozoic and Mesozoic rocks of the Geyikdağı and Bolkardağ nappes of the Taurides (e.g., Güngör, 2013), represents a Miocene extensional core complex, bounded by a top-to-the-east detachment of which the IB represents a supradetachment basin. Analogous structures may be seen in the core complex, where the Alasehir or Büyük Menderes detachments bound the central Menderes massif and have exhumed footwalls of similar dimension as the Sultandağları range (e.g., Çiftçi & Bozkurt, 2010; Gessner et al., 2001; Işık et al., 2003). The Yalvaç-Beyşehir valley may then be a second-order extensional feature in the doming footwall, equivalent to the Küçük Menderes graben (Seyitoğlu & Işık, 2009).

Typical core complexes are bound by low-angle detachment faults (Davis & Lister, 1988; Lister & Davis, 1989; Wernicke, 1981). Such low-angle detachment faults are initially high-angle normal faults and that due to doming and backrotating of the footwall upon fault motion become low angle (Buck, 1988; Wernicke & Axen, 1988). The modern range-bounding fault of the Sultandağları range is a high-angle normal fault, the Akşehir-Afyon fault zone (Figures 2 and 9e). This modern range-bounding normal fault may thus either be a high-angle normal fault cutting a low-angle detachment, or the range represents a fairly immature stage of core complex formation (Figure 9e). We stress that the inference that the Sultandağları range represents a Miocene core complex is a prediction that follows from our map-view restoration (Figures 9a–9c) based on paleomagnetic and structural constraints from the adjacent basin, and further evaluation of its exhumation history remains a subject for future field study.

6. Conclusions

In this study, we provide a paleomagnetic study of Miocene continental sediments in the heart and the eastern limb of the Isparta angle in southwest Turkey. Our results allow us to determine vertical axis rotations, within the context of the tectonic and geodynamic evolution of the Central Tauride region, and we illustrate the use of paleomagnetic constraints in estimating crustal extension by restoring tectonic rotations. Our main findings can be summarized as follows.

Four different rotational domains are distinguished in the continental basins that are located in the north and east of the Isparta angle: (1) The BB in the north recorded ~10° CCW rotation in Late Miocene-Pliocene, (2) the YB in the northern center shows a net 42° CW rotation since the Middle Miocene, (3) the IB in the east underwent ~27° CW rotation between the Early and Middle Miocene, followed by ~21° CCW rotation since the Middle Miocene, and (4) the Altınapa basin has a similar rotational history showing a ~26° CW rotation between the Early and Middle Miocene, followed by ~30° CCW rotation since the Middle Miocene. We attribute the additional ~9° CW rotation of the Altınapa basin to be caused by the normal relay ramp faults in the IB.

The 26–27° CW rotation must have happened before ~12 Ma that is the age of the angular unconformity, after which the Ilgın and Altınapa basins were subjected to ~20–30° CCW rotation caused by extensional deformation controlled by low- and/or high-angle normal faults. The large net ~42° CW rotation of the YB is in excess of the regional rotation between ~20 and 12 Ma that we attribute to lateral variations in normal slip along the four basin-bounding normal faults.

We attempt a first-order map-view restoration of the kinematic evolution of the region based on our new paleomagnetic constraints since the early Miocene. Restoring ~25° CW rotation accommodated by the northern limb of the orocline predicts up to ~50–60 km of extension in the core of the orocline and ~30–35 km of extension in the basins. The reconstruction generates an almost complete overlap between the Sultandağları footwall and the hanging wall basin blocks of the Altınapa-IB. This predicts that the Sultandağları range that exposes low-grade metamorphic rocks represents a Miocene extensional core complex. Our study highlights the view that the Neogene deformation history, and perhaps even active tectonics, may be strongly affected by the westward retreat of the Antalya slab.

Acknowledgments
Research for this paper was supported by ÖYP Research Fund of Turkish Government (BAP-08-11-DPT.2002 K120510) and TUBITAK (the Scientific and Technological Research Council of Turkey) International Postdoctoral Research Fellowship Programme (2219). D. J. J. v. H. was supported by NWO Vidi grant 864.11.004. Wout Krijgsman is thanked for sharing the original data of the Harami section with us. We thank Nuretdin Kaymakcı for his support and Murat Özkaptan, Erhan Gülyüz, Kıvanç Yücel, and Pınar Ertepınar for their help during fieldworks in 2010 and 2013. We thank John Piper and an anonymous reviewer for their constructive comments. The data used are listed in the references, figures, tables, and supporting information.

References

Advokaat, E. L., van Hinsbergen, D., Kaymakci, N., Vissers, R. L. M., & Hendriks, B. W. H. (2014). Late Cretaceous extension and Palaeogene rotation-related contraction in Central Anatolia recorded in the Ayhan-Büyükkışla basin. *International Geology Review*, *56*(15), 1813–1836. https://doi.org/10.1080/00206814.2014.954279

Altıner, D., Yılmaz, İ. Ö., Özgül, N., Akçar, N., Bayazıtoğlu, M., & Gaziulusoy, Z. E. (1999). High-resolution sequence stratigraphic correlation in the Upper Jurassic (Kimmeridgian)–Upper Cretaceous (Cenomanian) peritidal carbonate deposits (western Taurides, Turkey). *Geological Journal*, *34*(1-2), 139–158. https://doi.org/10.1002/(SICI)1099-1034(199901/06)34:1/2%3C139::AID-GJ818%3E3.0.CO;2-7

Andrew, T., & Robertson, A. H. (2002). The Beyşehir–Hoyran–Hadim Nappes: Genesis and emplacement of Mesozoic marginal and oceanic units of the northern Neotethys in southern Turkey. *Journal of the Geological Society*, *159*(5), 529–543. https://doi.org/10.1144/0016-764901-157

Barrier, E., & Vrielynck, B. (2008). Palaeotectonic maps of the Middle East: Tectono-sedimentary-palinspatic maps from Late Norian to Pliocene: *Paris*, *Commission for the Geological Map of the World* (*CGMW*)*/UNESCO* (http://www.ccgm.org) *Atlas of 14 maps*, scale 1:18,500,000.

Biggin, A. J., Van Hinsbergen, D. J., Langereis, C. G., Straathof, G. B., & Deenen, M. H. (2008). Geomagnetic secular variation in the Cretaceous Normal Superchron and in the Jurassic. *Physics of the Earth and Planetary Interiors*, *169*(1-4), 3–19.

Biryol, C. B., Beck, S. L., Zandt, G., & Özacar, A. A. (2011). Segmented African lithosphere beneath the Anatolian region inferred from teleseismic P-wave tomography. *Geophysical Journal International*, *184*(3), 1037–1057. https://doi.org/10.1111/j.1365-246X.2010.04910.x

Buck, W. R. (1988). Flexural rotation of normal faults. *Tectonics*, *7*(5), 959–973. https://doi.org/10.1029/TC007i005p00959

Çiftçi, N. B., & Bozkurt, E. (2010). Structural evolution of the Gediz Graben, SW Turkey: Temporal and spatial variation of the graben basin. *Basin Research*, *22*, 846–873.

Davis, G. A., & Lister, G. S. (1988). Detachment faulting in continental extension: Perspectives from the southwestern US Cordillera. In S. P. Clark Jr., B. C. Burchfiel, & J. Suppe (Eds.), *Processes in continental lithospheric deformation, Geological Society of America Special Paper* (Vol. 218, pp. 133–159).

Deenen, M. H. L., Langereis, C. G., van Hinsbergen, D. J. J., & Biggin, A. J. (2011). Geomagnetic secular variation and the statistics of palaeomagnetic directions. *Geophysical Journal International*, *186*(2), 509–520. https://doi.org/10.1111/j.1365-246X.2011.05050.x

Deenen, M. H. L., Langereis, C. G., van Hinsbergen, D. J. J., & Biggin, A. J. (2014). Erratum: Geomagnetic secular variation and the statistics of palaeomagnetic directions. *Geophysical Journal International*, *197*(1), 643. https://doi.org/10.1093/gji/ggu021

DeMets, C., Iaffaldano, G., & Merkouriev, S. (2015). High-resolution Neogene and Quaternary estimates of Nubia-Eurasia-North America plate motion. *Geophysical Journal International*, *203*(1), 416–427. https://doi.org/10.1093/gji/ggv277

Dewey, J. F., & Şengör, A. C. (1979). Aegean and surrounding regions: Complex multiplate and continuum tectonics in a convergent zone. *Geological Society of America Bulletin*, *90*(1), 84–92. https://doi.org/10.1130/0016-7606(1979)90%3C84:AASRCM%3E2.0.CO;2

Ergin, M., Aktar, M., Özalaybey, S., Tapirdamaz, M. C., Selvi, O., & Tarancıoglu, A. (2009). A high-resolution aftershock seismicity image of the 2002 Sultandağı-Çay earthquake (Mw = 6.2). *Turkey*. *Journal of Seismology*, *13*(4), 633–646. https://doi.org/10.1007/s10950-009-9155-1

Faccenna, C., Bellier, O., Martinod, J., Piromallo, C., & Regard, V. (2006). Slab detachment beneath eastern Anatolia: A possible cause for the formation of the North Anatolian fault. *Earth and Planetary Science Letters*, *242*(1-2), 85–97. https://doi.org/10.1016/j.epsl.2005.11.046

Fernandez-Blanco, D., Bertotti, G., & Çiner, T. A. (2013). Cenozoic tectonics of the Tuz Gölü basin (central Anatolia plateau, Turkey). *Turkish Journal of Earth Sciences*, *22*, 715–738. https://doi.org/10.3906/yer-1206-7

Gaina, C., Torsvik, T. H., van Hinsbergen, D. J. J., Medvedev, S., Werner, S. C., & Labails, C. (2013). The African plate: A history of oceanic crust accretion and subduction since the Jurassic. *Tectonophysics*, *604*, 4–25. https://doi.org/10.1016/j.tecto.2013.05.037

Gans, C. R., Beck, S. L., Zandt, G., Biryol, C. B., & Ozacar, A. A. (2009). Detecting the limit of slab break-off in central Turkey: New high-resolution Pn tomography results. *Geophysical Journal International*, *179*(3), 1566–1572. https://doi.org/10.1111/j.1365-246X.2009.04389.x

Garfunkel, Z., & Ron, H. (1985). Block rotation and deformation by strike-slip faults: 2. The properties of a type of macroscopic discontinuous deformation. *Journal of Geophysical Research*, *90*(B10), 8589–8602. https://doi.org/10.1029/JB090iB10p08589

Gessner, K., Ring, U., Johnson, C., Hetzel, R., Passchier, C. W., & Güngör, T. (2001). An active bivergent rolling-hinge detachment system: Central Menderes metamorphic core complex in western Turkey. *Geology*, *29*(7), 611–614. https://doi.org/10.1130/0091-7613(2001)029%3C0611:AABRHD%3E2.0.CO;2

Gibbs, A. D. (1983). Balanced cross-section construction from seismic sections in areas of extensional tectonics. *Journal of Structural Geology*, *5*(2), 153–160.

Granot, R. (2016). Palaeozoic oceanic crust preserved beneath the eastern Mediterranean. *Nature Geoscience*, *9*(9), 701–705. https://doi.org/10.1038/ngeo2784

Gülyüz, E., Kaymakci, N., Meijers, M. J. M., van Hinsbergen, D. J. J., Lefebvre, C., Vissers, R. L. M., et al. (2013). Late Eocene evolution of the Çiçekdağı basin (central Turkey): Syn-sedimentary compression during microcontinent–continent collision in central Anatolia. *Tectonophysics*, *602*(C), 286–299. https://doi.org/10.1016/j.tecto.2012.07.003

Güngör, T. (2013). Kinematics of the central Taurides during Neotethys closure and collision, the nappes in the Sultan Mountains, Turkey. *International Journal of Earth Sciences*, *102*(5), 1381–1402. https://doi.org/10.1007/s00531-012-0854-4

Gürer, D., & van Hinsbergen, D. J. J. (2018). Diachronous demise of the Neotethys Ocean as a driver for non-cylindrical orogenesis in Anatolia. *Tectonophysics*. https://doi.org/10.1016/j.tecto.2018.06.005

Gürer, D., van Hinsbergen, D. J. J., Maţenco, L., Corfu, F., & Cascella, A. (2016). Kinematics of a former oceanic plate of the Neotethys revealed by deformation in the Ulukışla basin (Turkey). *Tectonics*, *35*(10), 2385–2416. https://doi.org/10.1002/(ISSN)1944-9194

Gürer, D., van Hinsbergen, D. J. J., Özkaptan, M., Creton, I., Koymans, M. R., Cascella, A., & Langereis, C. G. (2018). Paleomagnetic constraints on the timing and distribution of Cenozoic rotations in central and eastern Anatolia. *Solid Earth*, *9*(2), 295–322. https://doi.org/10.5194/se-9-295-2018

Gürsoy, H., Piper, J. D. A., & Tatar, O. (2003). Neotectonic deformation in the western sector of tectonic escape in Anatolia: Palaeomagnetic study of the Afyon region, central Turkey. *Tectonophysics*, *374*(1-2), 57–79. https://doi.org/10.1016/S0040-1951(03)00346-9

Higgins, M., Schoenbohm, L. M., Brocard, G. Y., Kaymakci, N., Gosse, J. C., & Cosca, M. A. (2015). New kinematic and Geochronologic evidence for the quaternary evolution of the central Anatolian fault zone. *Tectonics*, *34*, 2118–2141. https://doi.org/10.1002/2015TC003864

Hüsing, S. K., Zachariasse, W. J., Van Hinsbergen, D. J., Krijgsman, W., Inceöz, M., Harzhauser, M. et al. (2009). Oligocene–Miocene basin evolution in SE Anatolia, Turkey: constraints on the closure of the eastern Tethys gateway. *Geological Society, London, Special Publications*, *311*(1), 107–132.

Işık, V., Seyitoglu, G., & Cemen, I. (2003). Ductile–brittle transition along the Alaşehir detachment fault and its structural relationship with the Simav detachment fault, Menderes massif, western Turkey. *Tectonophysics*, *374*(1–2), 1–18. https://doi.org/10.1016/S0040-1951(03)00275-0

Jackson, J. A. (1987). Active normal faulting and crustal extension. *Geological Society, London, Special Publications*, *28*(1), 3–17.

Jaffey, N., & Robertson, A. (2005). Non-marine sedimentation associated with Oligocene-recent exhumation and uplift of the central Taurus Mountains, S Turkey. *Sedimentary Geology*, *173*(1–4), 53–89. https://doi.org/10.1016/j.sedgeo.2003.11.025

Jarvis, G. T., & Mckenzie, D. P. (1980). Sedimentary basin formation with finite extension rates. *Earth and Planetary Science Letters*, *48*(1), 42–52. https://doi.org/10.1016/0012-821X(80)90168-5

Kalyoncuoğlu, Ü. Y., Elitok, Ö., Dolmaz, M. N., & Anadolu, N. C. (2011). Geophysical and geological imprints of southern Neotethyan subduction between Cyprus and the Isparta angle, SW Turkey. *Journal of Geodynamics*, *52*(1), 70–82. https://doi.org/10.1016/j.jog.2010.12.001

Keller, J., Jung, D., Burgath, K., & Wolff, F. (1977). Geologie und petrographie des Neogenen Kalkalkali-Vulkanismus von Konya (Erenler Dağ-Alaca Dağ-massiv, ZentralAnatolien). *Geologisches Jahrbuch Hessen*, *25*, 37–117.

Keskin, M. (2003). Magma generation by slab steepening and breakoff beneath a subduction-accretion complex: An alternative model for collision-related volcanism in eastern Anatolia, Turkey. *Geophysical Research Letters*, *30*(24), 8046. https://doi.org/10.1029/2003GL018019

Khair, K., & Tsokas, G. N. (1999). Nature of the Levantine (eastern Mediterranean) crust from multiple-source Werner deconvolution of Bouguer gravity anomalies. *Journal of Geophysical Research*, *104*(B11), 25,469–25,478. https://doi.org/10.1029/1999JB900228

Kirschvink, J. L. (1980). The least-square line and plane and the analysis of paleomagnetic data. *Geophysical Journal of the Royal Astronomical Society*, *62*(3), 699–718. https://doi.org/10.1111/j.1365-246X.1980.tb02601.x

Kissel, C., & Poisson, A. (1986). Étude paléomagnetique des formations néogènes du bassin d'Antalya (Taurides occidentales-Turquie*). Comptes Rendus Acadademie Science,* Paris 302, Série II, 711–716.

Kissel, C., & Poisson, A. (1987). Étude paléomagnetique préliminaire des formations cénozoïques des Bey Dağları (Taurides occidentales, Turquie). *Comptes Rendus Academie Science,* Paris 304 (Série II), 343–348.

Koç, A., Kaymakci, N., van Hinsbergen, D. J. J., & Kuiper, K. F. (2017). Miocene tectonic history of the central Tauride intramontane basins, and the paleogeographic evolution of the central Anatolian plateau. *Global and Planetary Change*, *158*, 83–102. https://doi.org/10.1016/j.gloplacha.2017.09.001

Koç, A., Kaymakci, N., van Hinsbergen, D. J. J., Kuiper, K. F., & Vissers, R. L. M. (2012). Tectono-sedimentary evolution and geochronology of the middle Miocene Altınapa basin, and implications for the Late Cenozoic uplift history of the Taurides, southern Turkey. *Tectonophysics*, *532–535*, 134–155.

Koç, A., Kaymakci, N., van Hinsbergen, D. J. J., & Vissers, R. L. M. (2016). A Miocene onset of the modern extensional regime in the Isparta angle: Constraints from the Yalvaç basin (southwest Turkey). *International Journal of Earth Sciences*, *105*(1), 369–398. https://doi.org/10.1007/s00531-014-1100-z

Koç, A., van Hinsbergen, D. J. J., Kaymakci, N., & Langereis, C. G. (2016). Late Neogene oroclinal bending in the central Taurides: A record of terminal eastward subduction in southern Turkey? *Earth and Planetary Science Letters*, *434*, 75–90. https://doi.org/10.1016/j.epsl.2015.11.020

Koçyiğit, A., & Özacar, A. A. (2003). Extensional Neotectonic regime through the NE edge of the outer Isparta angle, SW Turkey: New field and seismic data. *Turkish Journal of Earth Sciences*, *12*, 67–90.

Koçyiğit, A., & Saraç, G. (2000). Episodic graben formation and extensional neotectonic regime in west central Anatolia and the Isparta angle: A case study in the Akşehir-Afyon graben, Turkey. *Geological Society, London, Special Publications*, *173*(1), 405–421. https://doi.org/10.1144/GSL.SP.2000.173.01.19

Koymans, M. R., Langereis, C. G., Pastor-Galan, D., & van Hinsbergen, D. J. J. (2016). Paleomagnetism.org: An online multi-platform open source environment for paleomagnetic data analysis. *Computers & Geosciences*, *93*, 127–137. https://doi.org/10.1016/j.cageo.2016.05.007

Krijgsman, W., Duermeijer, C. E., Langereis, C. G., de Bruijn, H., Sarac, G., & Andriessen, P. A. M. (1996). Magnetic polarity stratigraphy of Upper Oligocene to Middle Miocene mammal-bearing continental deposits in central Anatolia (Turkey). *Newsletters in Stratigraphy*, *34*(1), 13–29. https://doi.org/10.1127/nos/34/1996/13

Larsen, P. H. (1988). Relay structures in a Lower Permian basement-involved extension system, East Greenland. *Journal of Structural Geology*, *10*(1), 3–8. https://doi.org/10.1016/0191-8141(88)90122-8

Li, S., Advokaat, E. L., van Hinsbergen, D. J., Koymans, M. R., Deng, C., & Zhu, R. (2017). Paleomagnetic constraints on the Mesozoic-Cenozoic paleolatitudinal and rotational history of Indochina and South China: Review and updated kinematic reconstruction. *Earth-Science Reviews*, *171*, 58–77. https://doi.org/10.1016/j.earscirev.2017.05.007

Lister, G. S., & Davis, G. A. (1989). The origin of metamorphic core complexes and detachment faults formed during Tertiary continental extension in the northern Colorado River region, USA. *Journal of Structural Geology*, *11*(1-2), 65–94.

Mackintosh, P. W., & Robertson, A. H. (2009). Structural and sedimentary evidence from the northern margin of the Tauride platform in south central Turkey used to test alternative models of Tethys during Early Mesozoic time. *Tectonophysics*, *473*(1-2), 149–172. https://doi.org/10.1016/j.tecto.2008.10.031

Martin, A. (2011). Double saloon door tectonics in the Japan Sea, Fossa Magna, and the Japanese Island arc. *Tectonophysics*, *498*(1-4), 45–65. https://doi.org/10.1016/j.tecto.2010.11.016

McFadden, P. L., & McElhinny, L. W. (1988). The combined analysis of remagnetization circles and direct observations in palaeomagnetism. *Earth and Planetary Science Letters*, *87*(1-2), 161–172. https://doi.org/10.1016/0012-821X(88)90072-6

McKenzie, D., & Jackson, J. (1983). The relationship between strain rates, crustal thickening, palaeomagnetism, finite strain and fault movements within a deforming zone. *Earth and Planetary Science Letters*, *65*(1), 182–202. https://doi.org/10.1016/0012-821X(83)90198-X

Meijers, M. J. M., van Hinsbergen, D. J. J., Dekkers, M. J., Altıner, D., Kaymakcı, N., & Langereis, C. G. (2011). Pervasive Paleogene remagnetization of the central Taurides fold-and-thrust belt (southern Turkey) and implications for rotations in the Isparta angle. *Geophysical Journal International*, *184*(3), 1090–1112. https://doi.org/10.1111/j.1365-246X.2010.04919.x

Menant, A., Jolivet, L., & Vrielynck, B. (2016). Kinematic reconstructions and magmatic evolution illuminating crustal and mantle dynamics of the eastern Mediterranean region since the Late Cretaceous. *Tectonophysics*, *675*, 103–140. https://doi.org/10.1016/j.tecto.2016.03.007

Morris, A., & Robertson, A. H. F. (1993). Miocene remagnetisation of carbonate platform and Antalya complex units within the Isparta angle, SW Turkey. *Tectonophysics*, *220*(1-4), 243–266. https://doi.org/10.1016/0040-1951(93)90234-B

Mullender, T. A. T., Frederichs, T., Hilgenfeldt, C., De Groot, L. V., Fabian, K., & Dekkers, M. J. (2016). Automated paleomagnetic and rock magnetic data acquisition with an in-line horizontal '2G' system. *Geochemistry, Geophysics, Geosystems*, *17*(9), 3546–3559. https://doi.org/10.1002/2016GC006436

Mullender, T. A. T., van Velzen, A. J., & Dekkers, M. J. (1993). Continuous drift correction and separate identification of ferromagnetic and paramagnetic contribution in thermomagnetic runs. *Geophysical Journal International*, *114*(3), 663–672. https://doi.org/10.1111/j.1365-246X.1993.tb06995.x

Nelson, M. R., & Jones, C. H. (1987). Paleomagnetism and crustal rotations along a shear zone, Las Vegas Range, southern Nevada. *Tectonics*, *6*(1), 13–33. https://doi.org/10.1029/TC006i001p00013

Okay, A. I. (1986). High-pressure/low-temperature metamorphic rocks of Turkey. In *Blueschists and eclogites*, *Geological Society of America Memoir* (Vol. 164, pp. 333–348). CO: The Geological Society of America.

Okay, A. I., Zattin, M., & Cavazza, W. (2010). Apatite fission-track data for Miocene Arabia–Eurasia collision. *Geology*, *38*(1), 35–38. https://doi.org/10.1130/G30234.1

Ori, G. G. (1989). Geologic history of the extensional basin of the Gulf of Corinth (? Miocene-Pleistocene), Greece. *Geology*, *17*(10), 918–921. https://doi.org/10.1130/0091-7613(1989)017%3C0918:GHOTEB%3E2.3.CO;2

Özer, E., Koc, H., & Ozsayar, T. Y. (2004). Stratigraphical evidence for the depression of the northern margin of the Menderes–Tauride block (Turkey) during the Late Cretaceous. *Journal of Asian Earth Sciences*, *22*(5), 401–412. https://doi.org/10.1016/S1367-9120(03)00084-1

Passier, H. D., De Lange, G. J., & Dekkers, M. J. (2001). Magnetic properties and geochemistry of the active oxidation front and the youngest sapropel in the eastern Mediterranean Sea. *Geophysical Journal International*, *145*(3), 604–614.

Peacock, D. C. P. (2002). Propagation, interaction and linkage in normal fault systems. *Earth-Science Reviews*, *58*(1–2), 121–142. https://doi.org/10.1016/S0012-8252(01)00085-X

Peacock, D. C. P., & Sanderson, D. J. (1994). Geometry and development of relay ramps in normal fault systems. *AAPG Bulletin*, *78*(2), 147–165.

Platzman, E. S., Tapirdamaz, C., & Sanver, M. (1998). Neogene anticlockwise rotation of central Anatolia (Turkey): preliminary palaeomagnetic and geochronological results. *Tectonophysics*, *299*(1-3), 175–189.

Pourteau, A., Candan, O., & Oberhänsli, R. (2010). High-pressure metasediments in central Turkey: Constraints on the Neotethyan closure history. *Tectonics*, *29*, TC5004. https://doi.org/10.1029/2009TC002650

Poyraz, S. A., Pınar, A., Özden, S., & Tunçer, M. K. (2014). Implications of 2007's earthquake activity in Eğirdir Lake (SW Anatolia) based on moment tensor solutions and inversion of stress state. *Pure and Applied Geophysics*, *171*(7), 1299–1309. https://doi.org/10.1007/s00024-013-0715-5

Reilinger, R., McClusky, S., Vernant, P., Lawrence, S., Ergintav, S., Cakmak, R., et al. (2006). GPS constraints on continental deformation in the Africa–Arabia–Eurasia continental collision zone and implications for the dynamics of plate interactions. *Journal of Geophysical Research*, *111*, BO5411. https://doi.org/10.1029/2005JB004051

Ricou, L. E., Argyriadis, I., & Marcoux, J. E. A. N. (1975). L'Axe Calcaire du Taurus, un alignement de fenetres arabo-africaines sous des nappes radiolaritiques, ophiolitiques et metamorphiques. *Bulletin de la Société géologique de France*, *7*(6), 1024–1044.

Robertson, A. (2004). Development of concepts concerning the genesis and emplacement of Tethyan ophiolites in the eastern Mediterranean and Oman regions. *Earth-Science Reviews*, *66*(3-4), 331–387. https://doi.org/10.1016/j.earscirev.2004.01.005

Ron, H., Freund, R., Garfunkel, Z., & Nur, A. (1984). Block rotation by strike-slip faulting: Structural and paleomagnetic evidence. *Journal of Geophysical Research*, *89*(B7), 6256–6270. https://doi.org/10.1029/JB089iB07p06256

Schildgen, T. F., Yıldırım, C., Cosentino, D., & Strecker, M. R. (2014). Linking slab break-off, Hellenic trench retreat, and uplift of the central and eastern Anatolian plateaus. *Earth-Science Reviews*, *128*, 147–168. https://doi.org/10.1016/j.earscirev.2013.11.006

Şengör, A. M. C., Özeren, S., Genç, T., & Zor, E. (2003). East Anatolian high plateau as a mantle-supported, north–south shortened domal structure. *Geophysical Research Letters*, *30*(24), 8045. https://doi.org/10.1029/2003GL017858

Şengör, A. M. C., & Yılmaz, Y. (1981). Tethyan evolution of Turkey: A plate tectonic approach. *Tectonophysics*, *75*(3–4), 181–190, 193–199, 203–241.

Seton, M., Müller, R. D., Zahirovic, S., Gaina, C., Torsvik, T. H., Shephard, G., et al. (2012). Global continental and ocean basin reconstructions since 200 Ma. *Earth-Science Reviews*, *113*(3–4), 212–270. https://doi.org/10.1016/j.earscirev.2012.03.002

Seyitoğlu, G., & Işık, V. (2009). Meaning of the Küçük Menderes graben in the tectonic framework of the central Menderes metamorphic core complex (western Turkey). *Geologica Acta*, *7*, 323–331. https://doi.org/10.1344/105.000001440

Stampfli, G., Marcoux, J., & Baud, A. (1991). Tethyan margins in space and time. *Palaeogeography, Palaeoclimatology, Palaeoecology*, *87*(1-4), 373–409. https://doi.org/10.1016/0031-0182(91)90142-E

Sussman, A. J., Butler, R. F., Dinares-Turell, J., & Vergés, J. (2004). Vertical-axis rotation of a foreland fold and implications for orogenic curvature: An example from the southern Pyrenees, Spain. *Earth and Planetary Science Letters*, *218*(3–4), 435–449. https://doi.org/10.1016/S0012-821X(03)00644-7

Tatar, O., Gürsoy, H., & Piper, J. D. A. (2002). Differential neotectonic rotations in Anatolia and the Tauride arc: Palaeomagnetic investigation of the Erenlerdağ volcanic complex and Isparta volcanic district, south–central Turkey. *Journal of the Geological Society*, *159*(3), 281–294. https://doi.org/10.1144/0016-764901-035

Tauxe, L. (2010). *Essentials of paleomagnetism*. Oakland, CA: University of California Press.

Tauxe, L., & Watson, G. S. (1994). The fold test: An eigen analysis approach. *Earth and Planetary Science Letters*, *122*(3-4), 331–341. https://doi.org/10.1016/0012-821X(94)90006-X

Taymaz, T., Tan, O., & Yolsal, S. (2004). Seismotectonics of western Turkey: A synthesis of source parameters and rupture histories of recent earthquakes. *Eos, Transactions American Geophysical Union*, *85*, 47.

Tiryakioğlu, İ., Floyd, M., Erdoğan, S., Gülal, G., Ergintav, S., McClusky, S., & Reilinger, R. (2013). GPS constraints on active deformation in the Isparta angle region of SW Turkey. *Geophysical Journal International*, *195*(3), 1455–1463. https://doi.org/10.1093/gji/ggt323

Torsvik, T. H., Van der Voo, R., Preeden, U., MacNiocaill, C., Steinberger, B., Doubrovine, P. V., et al. (2012). Phanerozoic polar wander, palaeogeography and dynamics. *Earth-Science Reviews*, *114*(3-4), 325–368. https://doi.org/10.1016/j.earscirev.2012.06.007

Trudgill, B., & Cartwright, J. (1994). Relay-ramp forms and normal-fault linkages, Canyonlands National Park, Utah. *Geological Society of America Bulletin*, *106*(9), 1143–1157. https://doi.org/10.1130/0016-7606(1994)106%3C1143:RRFANF%3E2.3.CO;2

van der Meer, D. G., van Hinsbergen, D. J. J., & Spakman, W. (2018). Atlas of the underworld: Slab remnants in the mantle, their sinking history, and a new outlook on lower mantle viscosity. *Tectonophysics*, *723*, 309–448. https://doi.org/10.1016/j.tecto.2017.10.004

van Hinsbergen, D. J. J., Dekkers, M. J., & Koç, A. (2010). Testing Miocene remagnetization of Bey Dağları: Timing and amount of Neogene rotations in SW Turkey. *Turkish Journal of Earth Sciences*, *19*, 123–156.

van Hinsbergen, D. J. J., Kaymakci, N., Spakman, W., & Torsvik, T. H. (2010). Reconciling the geological history of western Turkey with plate circuits and mantle tomography. *Earth and Planetary Science Letters*, *297*(3-4), 674–686. https://doi.org/10.1016/j.epsl.2010.07.024

van Hinsbergen, D. J. J., Maffione, M., Plunder, A., Kaymakcı, N., Ganerød, M., Hendriks, B. W., et al. (2016). Tectonic evolution and paleogeography of the Kırşehir block and the central Anatolian Ophiolites, Turkey. *Tectonics*, *35*, 983–1014. https://doi.org/10.1002/2015TC004018

van Hinsbergen, D. J. J., & Schmid, S. M. (2012). Map view restoration of Aegean-west Anatolian accretion and extension since the Eocene. *Tectonics*, *31*, TC5005. https://doi.org/10.1029/2012TC003132

Wernicke, B. (1981). Low-angle normal faults in the Basin and Range province: Nappe tectonics in an extending orogen. *Nature*, *291*(5817), 645–648. https://doi.org/10.1038/291645a0

Wernicke, B., & Axen, G. J. (1988). On the role of isostasy in the evolution of normal fault systems. *Geology*, *16*(9), 848–851. https://doi.org/10.1130/0091-7613(1988)016%3C0848:OTROII%3E2.3.CO;2

Zijderveld, J. D. A. (1967). A. C. demagnetization of rocks: Analysis of results. In D. W. Collinson, K. M. Creer, & S. K. Runcorn (Eds.), *Methods in palaeomagnetism* (pp. 254–286). Amsterdam: Elsevier.